Electronic Supplementary Information

Fully alternating and regioselective ring-opening copolymerization of phthalic anhydride with epoxides using highly active metal-free lewis pairs as a Catalyst

Anjaneyulu K, [†] Sreenath Pappuru[†] and Debashis Chakraborty *

Organometallic and Polymer Chemistry Lab, Department of Chemistry, IIT-Madras, Chennai-600036, Tamil Nadu, India.

* Corresponding author

Prof. Debashis Chakraborty (dchakraborty@iitm.ac.in)

Figure S1. ^{1}H NMR spectrum ($CDCl_3$, 400 MHz, 298K) of P(PA-*alt*-CHO) copolymer derived by the action of $B(C_2H_5)_3$ and PPNCl ($B(C_2H_5)_3$/PPNCl/PA/CHO = 2/1/200/200, Table 1 entry 3).

Figure S2. ^{13}C $\{^{1}H\}$ NMR spectrum ($CDCl_3$, 100 MHz, 298K) of P(PA-*alt*-CHO) copolymer derived by the action of $B(C_2H_5)_3$ and PPNCl ($B(C_2H_5)_3$/PPNCl/PA/CHO = 2/1/200/200, Table 1 entry 3).

Figure S3. ^{1}H NMR spectrum ($CDCl_3$, 400 MHz, 298K) of P(PA-*alt*- *t*BGE) copolymer derived by the action of $B(C_2H_5)_3$ and PPNCl ($B(C_2H_5)_3$/PPNCl/PA/*t*BGE = 2/1/200/200, Table 2 entry 8).

Figure S4. ^{13}C $\{^{1}H\}$ NMR spectrum ($CDCl_3$, 100 MHz, 298K) of P(PA-*alt*- *t*BGE) copolymer derived by the action of $B(C_2H_5)_3$ and PPNCl ($B(C_2H_5)_3$/PPNCl/PA/*t*BGE = 2/1/200/200, Table 2 entry 8).

Figure S5. Regiostructures of P(PA-*alt*- *t*BGE) polyesters: tail-to-tail (TT), head-to-tail (HT), and head-to-head (HH) junctions, Table 2 entry 8.

Figure S6. ^{1}H NMR spectrum ($CDCl_3$, 400 MHz, 298K) of P(PA-*alt*-BO) copolymer derived by the action of $B(C_2H_5)_3$ and PPNCl ($B(C_2H_5)_3$/PPNCl/PA/BO = 2/1/200/200, Table 2 entry 14).

Figure S7. ^{13}C $\{^{1}H\}$ NMR spectrum ($CDCl_3$, 100 MHz, 298K) of P(PA-*alt*-BO) copolymer derived by the action of $B(C_2H_5)_3$ and PPNCl ($B(C_2H_5)_3$/PPNCl/PA/BO = 2/1/200/200, Table 2 entry 14).

Figure S8. Regiostructures of polyesters: tail-to-tail (TT), head-to-tail (HT), and head-to-head (HH) junctions, Table 2 entry 14.

Figure S9. ^{1}H NMR spectrum ($CDCl_3$, 400 MHz, 298K) of P(PA-*alt*-CHO) copolymer derived by the action of $B(C_2H_5)_3$ and DMAP ($B(C_2H_5)_3$/DMAP/PA/CHO = 2/1/100/100, Table 1 entry 8).

Figure S10. ^{13}C $\{^{1}H\}$ NMR spectrum ($CDCl_3$, 100 MHz, 298K) of P(PA-*alt*-CHO) copolymer derived by the action of $B(C_2H_5)_3$ and DMAP ($B(C_2H_5)_3$/DMAP/PA/CHO = 2/1/100/100, Table 1 entry 8).

Figure S11. ^{1}H NMR spectrum ($CDCl_3$, 400 MHz, 298K) of P(PA-*alt*-*t*BGE) copolymer derived by the action of $B(C_2H_5)_3$ and DMAP ($B(C_2H_5)_3$/DMAP/PA/*t*BGE = 2/1/100/100, Table 2 entry 12).

Figure S12. ^{13}C $\{^{1}H\}$ NMR spectrum ($CDCl_3$, 100 MHz, 298K) of P(PA-*alt*-*t*BGE) copolymer derived by the action of $B(C_2H_5)_3$ and DMAP ($B(C_2H_5)_3$/DMAP/PA/*t*BGE = 2/1/100/100, Table 2 entry 12).

Figure S13. ^{1}H NMR spectrum ($CDCl_3$, 400 MHz, 298K) of P(PA-*alt*-CHO) copolymer derived by the action of $Al(CH)_3$ and PPNCl ($Al(CH)_3$/ PPNCl/PA/CHO = 2/1/200/200, Table 1 entry 13).

Figure S14. ^{13}C $\{^{1}H\}$ NMR spectrum ($CDCl_3$, 100 MHz, 298K) of P(PA-*alt*-CHO) copolymer derived by the action of $Al(CH)_3$ and PPNCl ($Al(CH)_3$/ PPNCl/PA/CHO = 2/1/200/200, Table 1 entry 13).

Figure S15. ^{1}H NMR spectrum ($CDCl_3$, 400 MHz, 298K) of P(PA-*alt*-CHO) copolymer derived by the action of Et_2Zn and PPNCl (Et_2Zn/ PPNCl/PA/CHO = 2/1/200/200, Table 1 entry 17).

Figure S16. ^{1}H NMR spectrum ($CDCl_3$, 400 MHz, 298K) of P(PA-*alt*-CHO) copolymer derived by the action of $^{n}Bu_2Mg$ and PPNCl ($^{n}Bu_2Mg$/PPNCl/PA/CHO = 2/1/200/200, Table 1 entry 20).

Figure S17. ^{13}C $\{^{1}H\}$ NMR spectrum ($CDCl_3$, 100 MHz, 298K) of P(PA-*alt*-CHO) copolymer derived by the action of $^{n}Bu_2Mg$ and PPNCl ($^{n}Bu_2Mg$/PPNCl/PA/CHO = 2/1/200/200, Table 1 entry 20).

Figure S18. GPC trace of purified product of entry 4 in Table 2.

Figure S19. GPC trace of purified product of entry 5 in Table 2.

Figure S20. GPC trace of purified product of entry 6 in Table 2.

Figure S21. GPC trace of purified product of entry 7 in Table 2.

Figure S22. GPC trace of purified product of entry 8 in Table 2.

Figure S23. GPC trace of purified product of entry 14 in Table 2.

Figure S24. GPC trace of purified product of entry 7 in Table 1.

Figure S25. GPC trace of purified product of entry 13 in Table 1.

Figure S26. GPC trace of purified product of entry 20 in Table 1.

Figure S27. MALDI-TOF MS spectrum of the low-molecular-weight P(PA-*alt*-*t*BGE) polyester synthesized by the catalysis of TEB/PPNCl-based LP.

Figure S28. MALDI-TOF MS spectrum of the low-molecular-weight P(PA-*alt*-CHO) polyester synthesized by the catalysis of TEB/PPNCl-based LP.

Figure S29. MALDI-TOF MS spectrum of the low-molecular-weight P(PA-*alt*-CHO) polyester synthesized by the catalysis of TEB/DMAP-based LP.

Figure S30. MALDI-TOF MS spectrum of the low-molecular-weight P(PA-*alt*-*t*BGE) polyester synthesized by the catalysis of TEB/DMAP-based LP.

Figure S31. (1) ^{1}H NMR ($CDCl_3$, 400 MHz, 298K) spectra of *t*BGE activation by TEB/DMAP pair; (2) ^{1}H NMR spectra of *t*BGE activation by TEB/TBD pair; (3) ^{1}H NMR spectra of *t*BGE activation by TEB/DBU pair; (Inset figure shows the chemical shifts of the H^a and H^b signals of neat *t*BGE (2.75 and 2.57 ppm).

Figure S32. Proposed cooperative mechanism for the zwitter ionic copolymerization of epoxides and PA catalyzed by $B(C_2H_5)_3$/DMAP-based Lewis pair.

Figure S33. Overlap of ^{1}H NMR monitoring of copolymerization of *t*BGE and PA catalyzed by $B(C_2H_5)_3$/PPNCl-based Lewis pair ($B(C_2H_5)_3$/PPNCl/PA/*t*BGE = 2/1/200/200, Table 2 entry 8).

Figure S34. ^{1}H NMR spectra ($CDCl_3$, 400 MHz, 298K) of P(PA-*alt*- *t*BGE)copolymer before and after deprotection of ^{t}Bu groups.

Figure S35. Representative ^{13}C NMR spectra ($CDCl_3$, 100 MHz, 298K) of P(PA-*alt*- *t*BGE) copolymer before and after deprotection of ^{t}Bu groups.

Figure S36. GPC curves of purified products of before and after deprotection.

Figure S37. Plot of M_n and M_w/M_n *vs.* PA conversion using Et_3B and PPNCl as catalyst at initiator/monomers ratio, Et_3B/ PPNCl/PA/*t*BGE = 2/1/200/200.

Figure S38. DSC trace (heating rate: 10 °C/min, 2nd scan) of P(PA-*alt*-CHO) copolymer derived by the action of Et_3B and PPNCl (Et_3B/ PPNCl/PA/CHO = 2/1/200/200, Table 2 entry 4).

Figure S39. DSC trace (heating rate: 10 °C/min, 2nd scan) of P(PA-*alt*-*t*BGE) copolymer derived by the action of Et_3B and PPNCl (Et_3B/ PPNCl/PA/*t*BGE = 2/1/200/200, Table 2 entry 8).

Figure S40. DSC trace (heating rate: 10 °C/min, 2nd scan) of P(PA-*alt*-BO) copolymer derived by the action of Et_3B and PPNCl (Et_3B/ PPNCl/PA/BO = 2/1/200/200, Table 2 entry 14).

Figure S41. DSC trace (heating rate: 10 °C/min, 2nd scan) of P(PA-*alt*-CHO) copolymer derived by the action of $Al(CH)_3$ and PPNCl ($Al(CH)_3$/PPNCl/PA/CHO = 2/1/200/200, Table 1 entry 13).

Figure S42. DSC trace (heating rate: 10 °C/min, 2nd scan) of P(PA-*alt*-CHO) copolymer derived by the action of $^nBu_2Mg$ and PPNCl ($^nBu_2Mg$/PPNCl/PA/CHO = 2/1/200/200, Table 1 entry 20).

Figure S43. DSC trace (heating rate: 10 °C/min, 2nd scan) of P(PA-*alt*-CHO) copolymer derived by the action of Et_3B and DMAP (Et_3B / DMAP/PA/CHO = 2/1/200/200, Table 1 entry 7).

Figure S44. DSC trace (heating rate: 10 °C/min, 2nd scan) of P(PA-*alt*-*t*BGE) copolymer derived by the action of Et_3B and DMAP (Et_3B / DMAP/PA/*t*BGE = 2/1/200/200, Table 2 entry 11).

Figure S45. TGA and DTG curves of P(PA-*alt*-CHO) copolymer derived by the action of Et_3B and PPNCl (Et_3B/ PPNCl/PA/CHO = 2/1/200/200, Table 2 entry 4).

Figure S46. TGA and DTG curves of P(PA-*alt*-*t*BGE) copolymer derived by the action of Et_3B and PPNCl (Et_3B/ PPNCl/PA/*t*BGE = 2/1/200/200, Table 2 entry 8).

Figure S47. TGA and DTG curves of P(PA-*alt*-BO) copolymer derived by the action of Et_3B and PPNCl (Et_3B/ PPNCl/PA/BO = 2/1/200/200, Table 2 entry 14).

Figure S48. TGA and DTG curves of P(PA-*alt*-CHO) copolymer derived by the action of $Al(CH)_3$ and PPNCl ($Al(CH)_3$/PPNCl/PA/CHO = 2/1/200/200, Table 1 entry 13).

Figure S49. TGA and DTG curves of P(PA-*alt*-CHO) copolymer derived by the action of Et_2Zn and PPNCl (Et_2Zn/PPNCl/PA/CHO = 2/1/200/200, Table 1 entry 17).

EXPERIMENTAL DETAILS

Materials, reagents and methods used. Monomers for polymerization *i.e.* pthalic anhydride (PA), cyclohexene oxide (CHO) and *tert*-butyl glycidyl ether (*t*BGE), Lewis acids (Et_3B, $Al(CH)_3$, Et_2Zn and $^nBu_2Mg$) and Lewis bases (PPNCl, DMAP, DBU and TBD) were purchased from Aldrich. CHO, *t*BGE and DBU were dried over CaH_2 overnight, vacuum-distillated, and stored in the glovebox for further use. PA was sublimed twice prior to use. The epoxide monomer, 2-benzyloxirane, BO was synthesized by slightly modifying the published procedure.[1] The deuterated solvent for NMR studies *i.e* $CDCl_3$ was acquired from Aldrich and purified by distilling over calcium hydride then stored in a glove box. The common reagents, common solvents were acquired locally and purified by usual methods. Toluene was dried by refluxing over sodium/benzophenone for at least 24 h and freshly distilled prior to use. All manipulations for the preparation of polyesters were carried out using either standard Schlenk techniques or glovebox techniques under a dry argon atmosphere. All ^1H and ^{13}C NMR and 2D NMR spectra were recorded on a Bruker Avance 400 MHz or 500 MHz spectrometers with chemical shifts given in parts per million (ppm) using residual solvent peak at 7.26 ppm as reference in the case of $CDCl_3$. Differential scanning calorimetry (DSC) for polymers were recorded using Perkin Elmer Q200 MDSC from TA instrument with RCS cooling accessory calibrated with indium at a rate of 10 ^oC min^{-1}, under continuous flow of nitrogen (50 mL min^{-1}), using aluminium capsules (typically 10mg of polymer). The thermograms were recorded according to the following cycles: -40 ^oC to +600 ^oC at 10 ^oC min^{-1}; +600 ^oC to -40 ^oC at 10 ^oC min^{-1}. Elemental analyses were performed using a Perkin Elmer Series 11 analyzer. MALDI-TOF MS spectra were recorded on a Bruker Daltonics instrument. We have used two matrix namely 2,5-dihydroxybenzoic acid (2,5-DHB) (Aldrich) and trans-2-[3-(4-t-butyl-phenyl)-2-methyl-2-propenylidene]

malononitrile (DCTB) (Aldrich) in different combinations for better ionization of polymer samples in MALDI-TOF MS spectrum. DHB matrix dissolved in TA30 solvent (30:70 [v/v] acetonitrile : 0.1% TFA in water) at a concentration of 40 $mg \cdot mL^{-1}$. The polymer samples were dissolved in THF at a concentration of 1 $mg \cdot mL^{-1}$. Solutions of matrix and polymer were mixed in a volume ratio of 2:1, respectively. The mixed solution was hand-spotted on a stainless steel MALDI target and left to dry. Spectra were recorded (Figure 5 and Figure S29) in both the linear and reflector mode. For other samples DCTB matrix was dissolved in THF at a concentration of 40 $mg \cdot mL^{-1}$. The cationization salt used was potassium trifluoroacetate/NaOAc (Aldrich) and dissolved in THF at a concentration of 5 $mg \cdot mL^{-1}$. The polymer samples were dissolved in THF at a concentration of 1 $mg \cdot mL^{-1}$. Solutions of matrix, salt and polymer were mixed in a volume ratio of 10:1:5, respectively. The procedure of spotting and method of characterization is similar to that described for above samples.[3] Molecular weights (M_n and M_w) and the MWDs (M_w/M_n) of polymer samples were determined by GPC instrument with Waters 510 pump and Waters 410 or 2414 differential refractometer as the detector. Three columns, namely WATERS STRYGEL-HR5, STRYGEL-HR4 and STRYGEL-HR3, each of dimensions (7.8 × 300 mm), were connected in series. Measurements were done in THF at 27 °C. Number average molecular weights (M_n) and MWDs (M_w/M_n) of polymers were measured relative to polystyrene standards.

Typical procedure for the alternating copolymerization of PA and variuos epoxides using Et_3B/PPNCl.

A dry schlenk tube containing in 2.5 mL of dry toluene under argon atmosphere was kept in a glove box and used as the reaction vessel. In a typical experiment (Table 1, entry 3), PA (2.96 g, 20 mmol), CHO (1.96 g, 20 mmol), Et_3B (0.2 mL, 0.2 mmol) and the PPNCl (57 mg, 0.1 mmol) at 200/200/2/1 ratio of monomers to Lewis pair were introduced to this vessel.

The schlenk tube was closed with a stopper and made air-tight using Teflon tape. The reaction vessel was then taken out side from glove box and immersed in an oil bath maintained at 100 °C and stirred over the appropriate period of time. The polymerization reaction was then quenched upon addition of an acetic acid solution (0.05 mL of a 1.6 mol L^{-1} solution in toluene). The reaction mixture was concentrated to dryness under vacuum, and the conversion of both monomers was determined by ^{1}H NMR analysis of the small aliquot from the residue in $CDCl_3$. The crude polymer was next dissolved in minimum amount of dichloromethane and precipitated by adding excess of cold methanol. The precipitate was filtered and dried under vacuum to a constant weight. The final copolymers were then analyzed by ^{1}H and ^{13}C NMR, GPC, MALDI-TOF MS, DSC and TGA experiments.

Deprotection of poly(*t*BGE-*alt*-PA).

Poly(*t*BGE-*alt*-MA) copolymer (Table 2, entry 8, 1.2 g, with 99 unit % of *t*BuGE) was dissolved in dry dichloromethane (2 mL) and trifluoroacetic acid (TFA) (8 mL) was added to the system to hydrolyse the poly-*t*BGE block. The solution was stirred at room temperature for 8 h. The polymer was isolated by following the literature method.[2] The excess acid was removed via vacuum pump. The crude product was dissolved in chloroform (40 mL) and washed three times with saturated sodium carbonate solution (20 mL). The organic phase was dried over sodium sulfate, and the solvent was evaporated. The polymer was dried under vacuum overnight. Yield: 95%.

References

1 X.-H. Zhang, R.-J. Wei, Y.-Y. Zhang, B.-Y. Du and Z.-Q. Fan, *Macromolecules*, 2015, **48**, 536-544.

2 M. Backes, L. Messager, A. Mourran, H. Keul and M. Moeller, *Macromolecules*, 2010, **43**, 3238-3248.

3 S. Huijser, G. D. Mooiweer, R. van der Hofstad, B. B. P. Staal, J. Feenstra, A. M. van Herk, C. E. Koning and R. Duchateau, *Macromolecules*, 2012, **45**, 4500-4510.

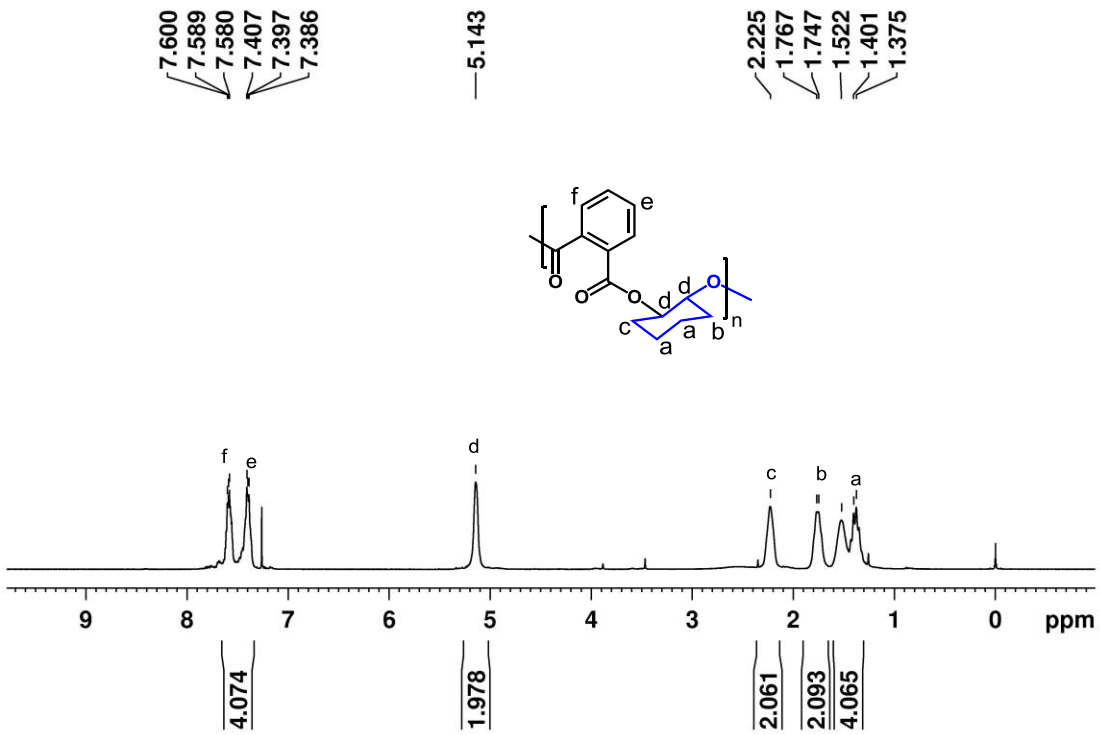

Figure S1. ^{1}H NMR spectrum ($CDCl_3$, 400 MHz, 298K) of P(PA-*alt*-CHO) copolymer derived by the action of $B(C_2H_5)_3$ and PPNCl ($B(C_2H_5)_3$/PPNCl/PA/CHO = 2/1/200/200, Table 1 entry 3).

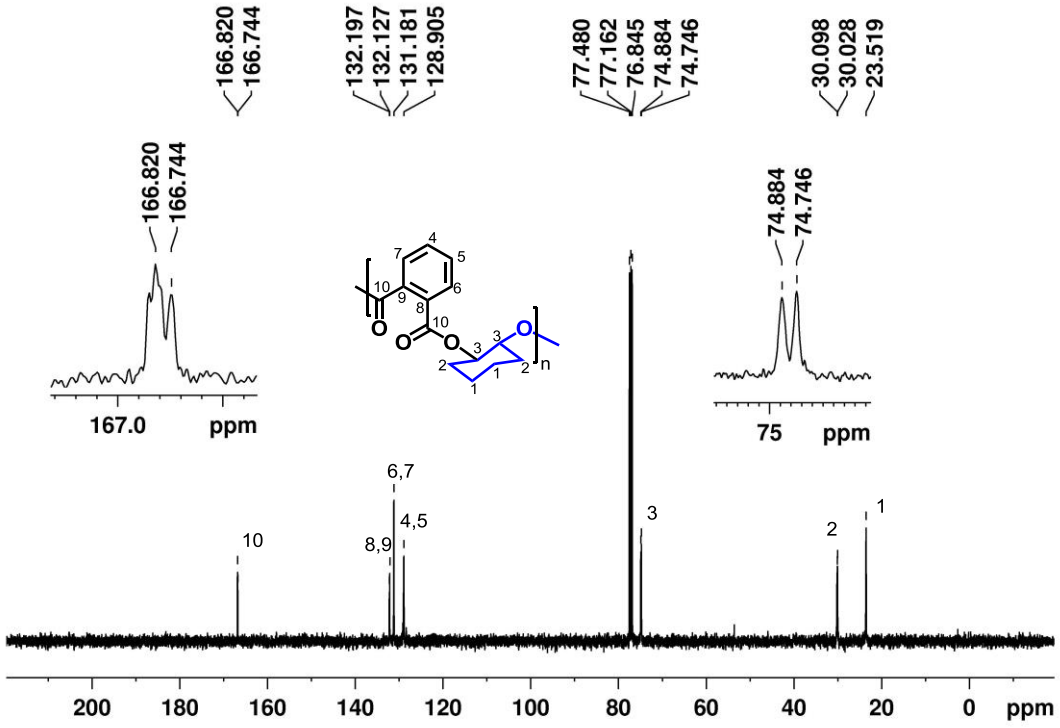

Figure S2. ^{13}C {^{1}H} NMR spectrum ($CDCl_3$, 100 MHz, 298K) of P(PA-*alt*-CHO) copolymer derived by the action of $B(C_2H_5)_3$ and PPNCl ($B(C_2H_5)_3$/PPNCl/PA/CHO = 2/1/200/200, Table 1 entry 3).

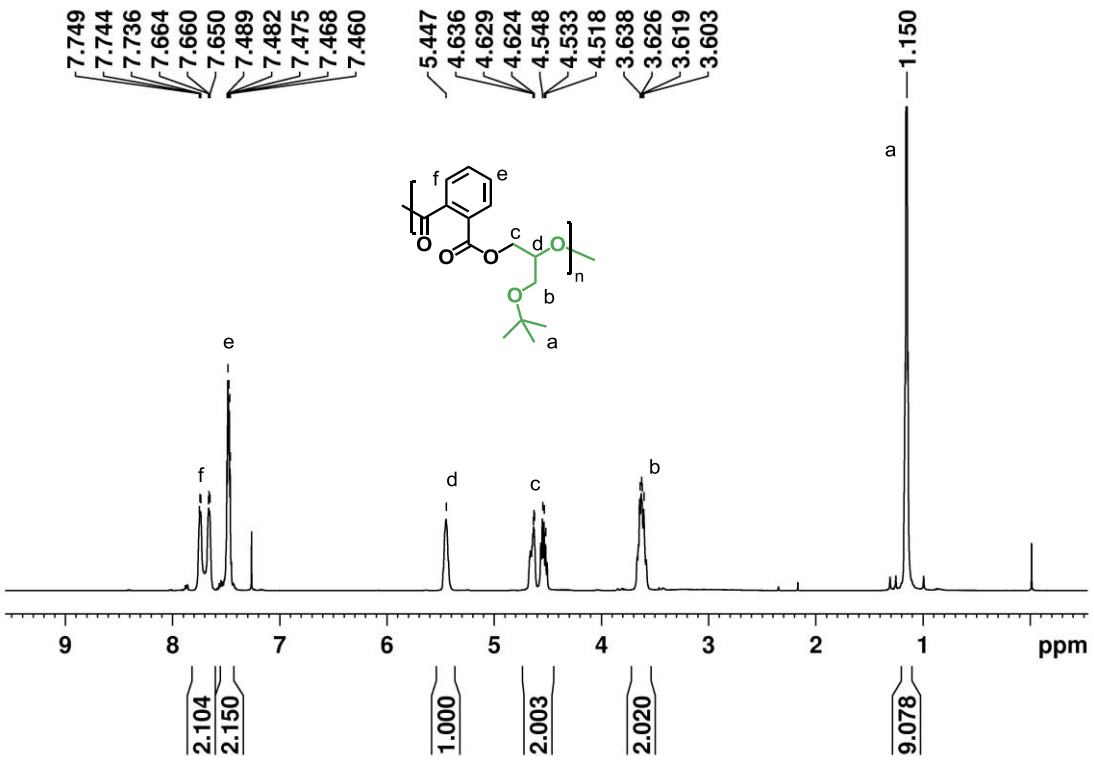

Figure S3. ^{1}H NMR spectrum ($CDCl_3$, 400 MHz, 298K) of P(PA-*alt*- *t*BGE) copolymer derived by the action of $B(C_2H_5)_3$ and PPNCl ($B(C_2H_5)_3$/PPNCl/PA/*t*BGE = 2/1/200/200, Table 2 entry 8).

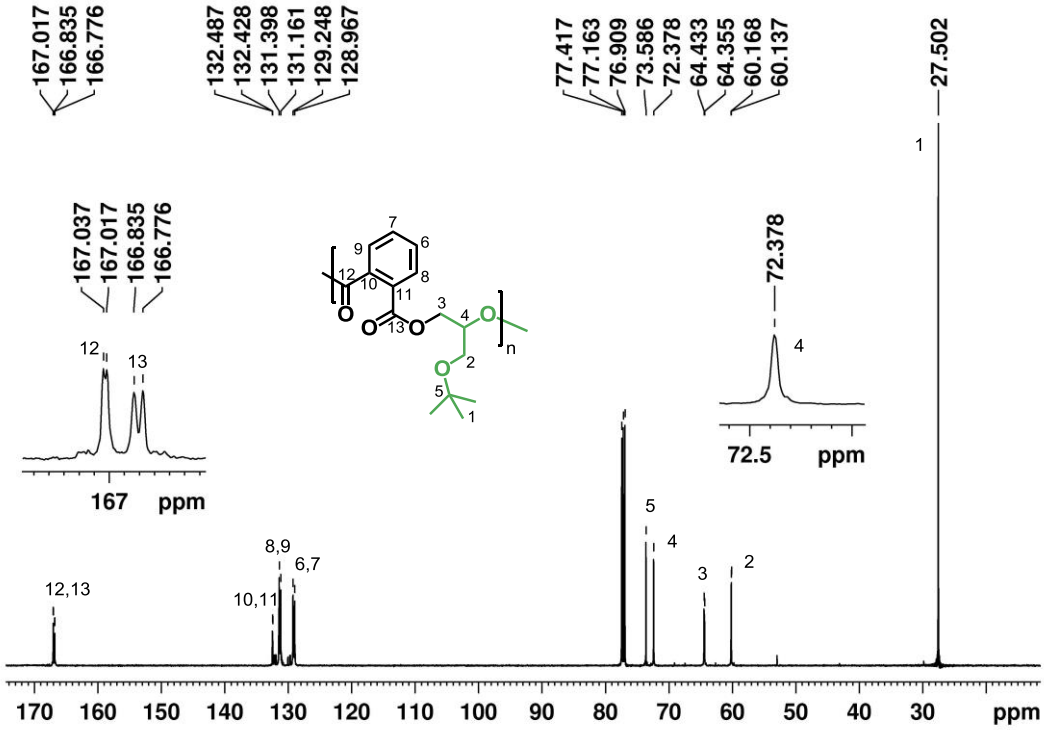

Figure S4. ^{13}C {^{1}H} NMR spectrum ($CDCl_3$, 100 MHz, 298K) of P(PA-*alt*- *t*BGE) copolymer derived by the action of $B(C_2H_5)_3$ and PPNCl ($B(C_2H_5)_3$/PPNCl/PA/*t*BGE = 2/1/200/200, Table 2 entry 8).

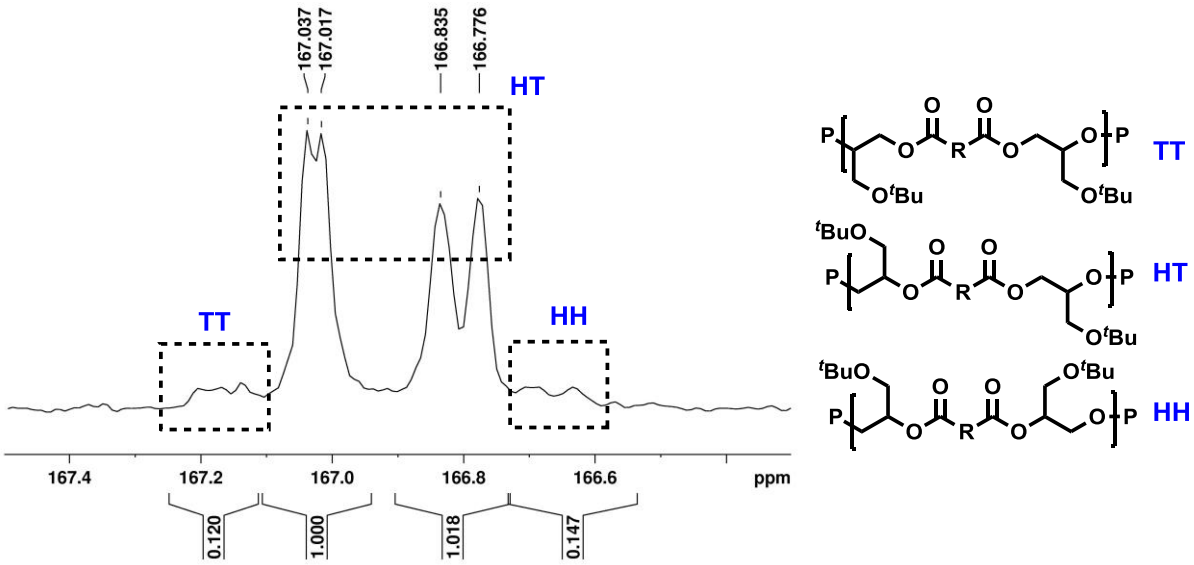

Figure S5. Regiostructures of P(PA-*alt*- *t*BGE) polyesters: tail-to-tail (TT), head-to-tail (HT), and head-to-head (HH) junctions, Table 2 entry 8.

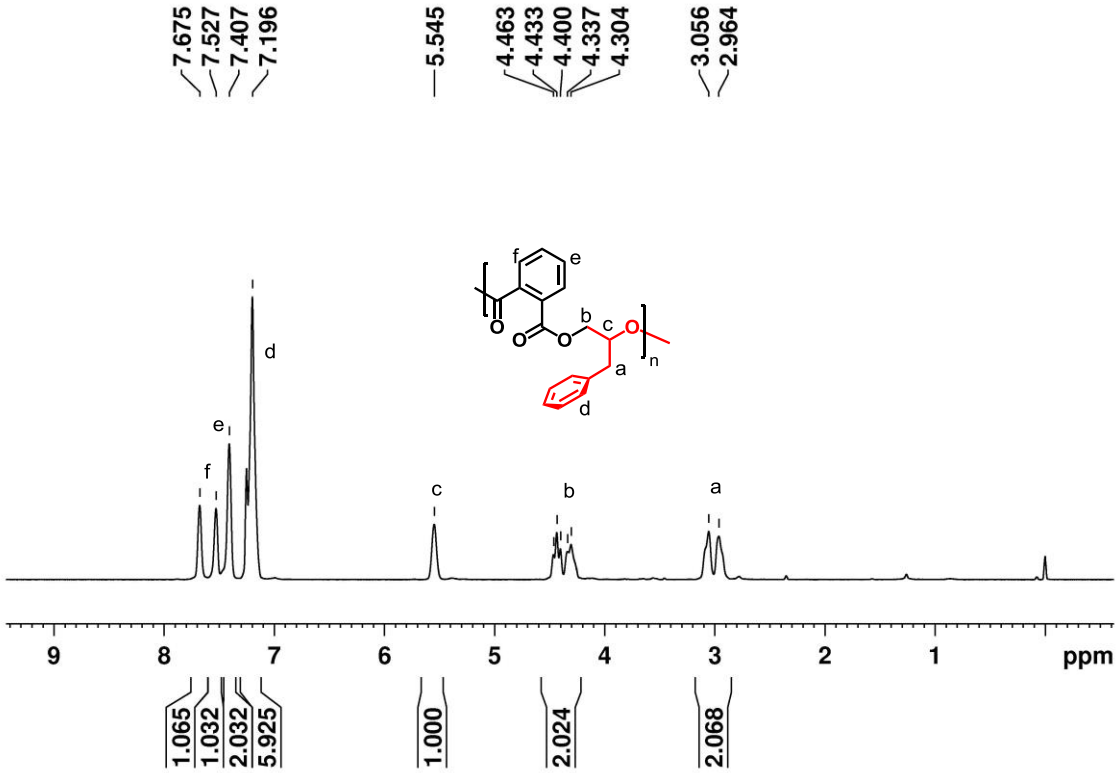

Figure S6. ^{1}H NMR spectrum ($CDCl_3$, 400 MHz, 298K) of P(PA-*alt*-BO) copolymer derived by the action of $B(C_2H_5)_3$ and PPNCl ($B(C_2H_5)_3$/PPNCl/PA/BO = 2/1/200/200, Table 2 entry 14).

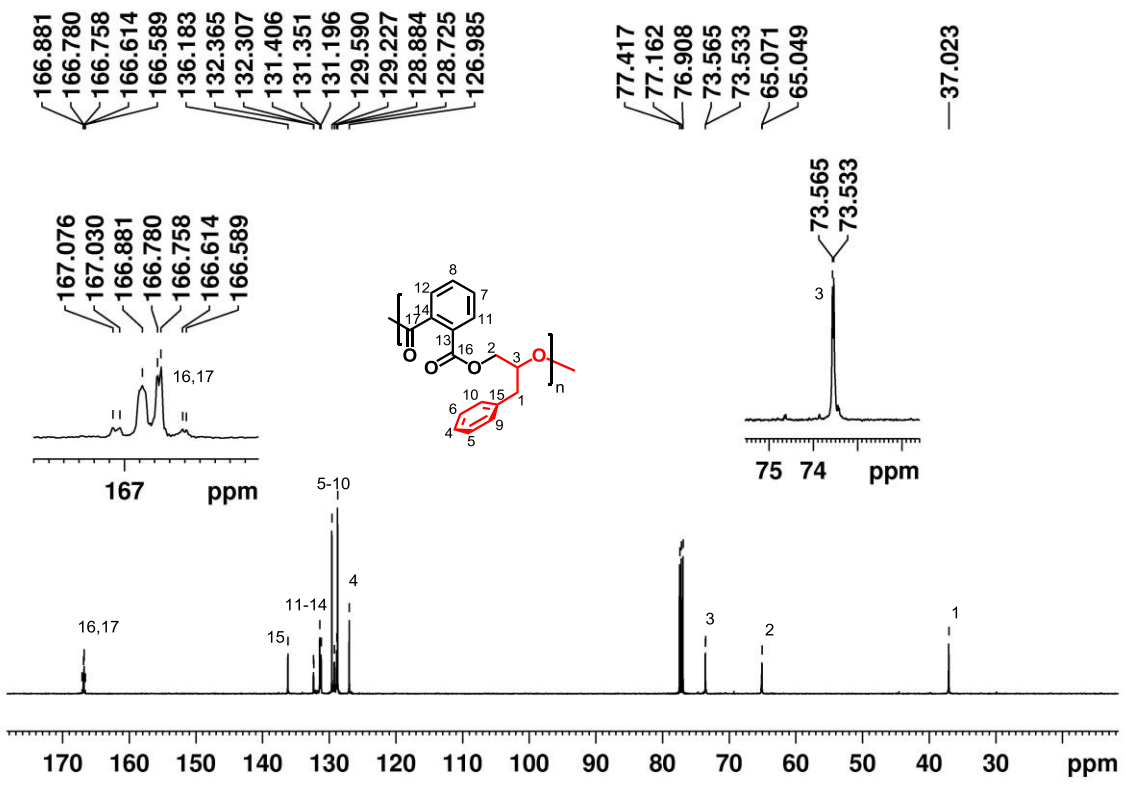

Figure S7. ^{13}C $\{^{1}H\}$ NMR spectrum ($CDCl_3$, 100 MHz, 298K) of P(PA-*alt*-BO) copolymer derived by the action of $B(C_2H_5)_3$ and PPNCl ($B(C_2H_5)_3$/PPNCl/PA/BO = 2/1/200/200, Table 2 entry 14).

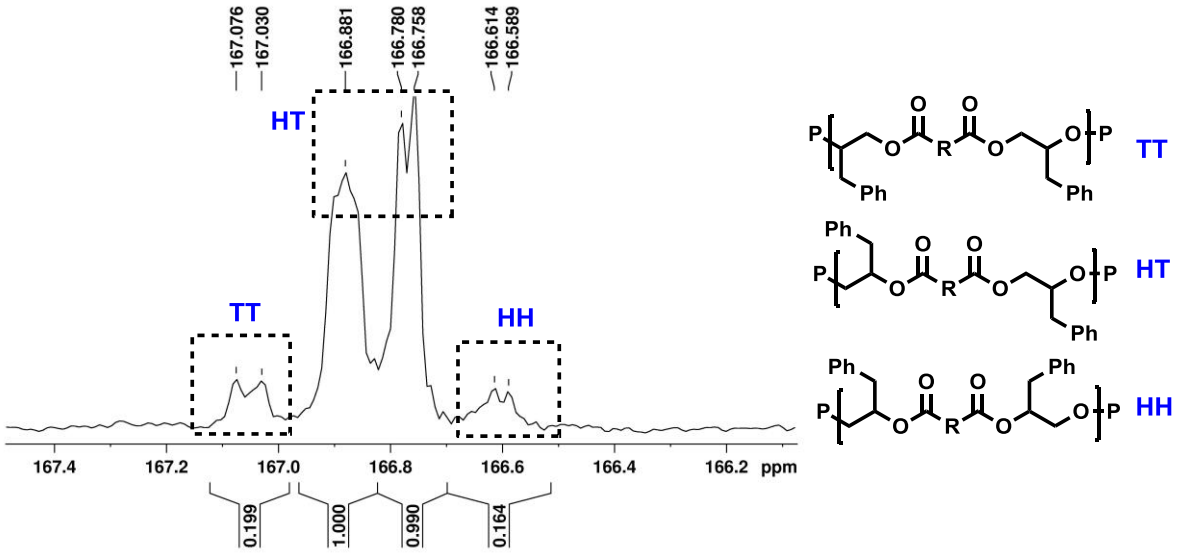

Figure S8. Regiostructures of polyesters: tail-to-tail (TT), head-to-tail (HT), and head-to-head (HH) junctions, Table 2 entry 14.

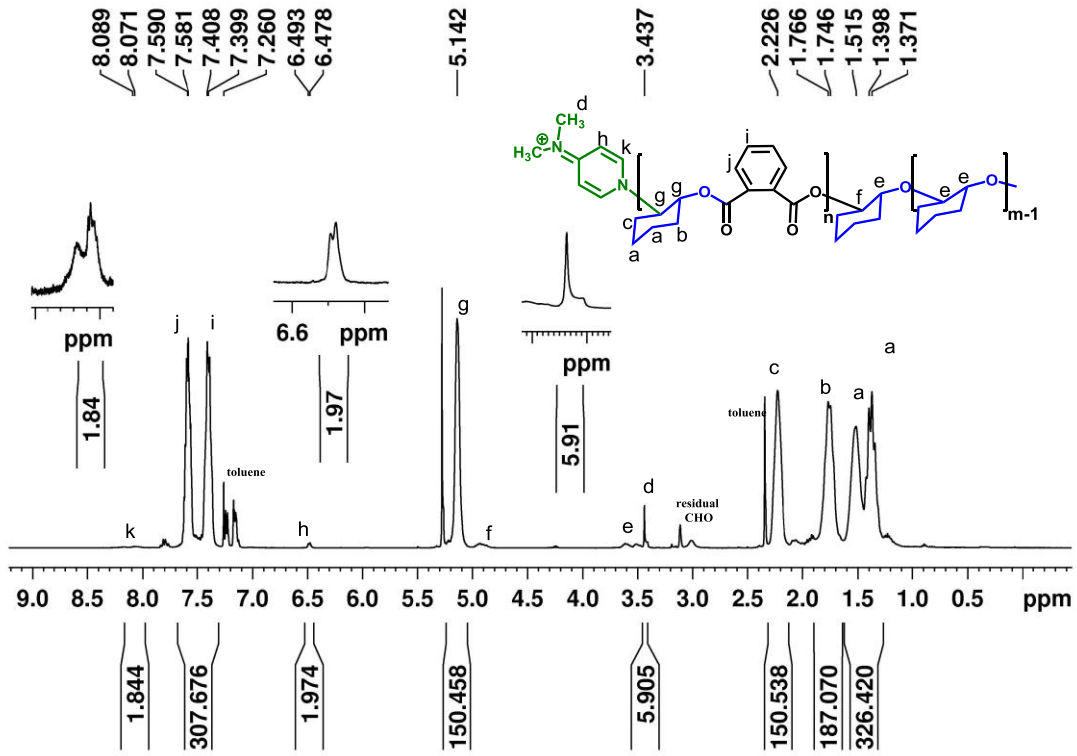

Figure S9. ^{1}H NMR spectrum ($CDCl_3$, 400 MHz, 298K) of P(PA-*alt*-CHO) copolymer derived by the action of $B(C_2H_5)_3$ and DMAP ($B(C_2H_5)_3$/DMAP/PA/CHO = 2/1/100/100, Table 1 entry 8).

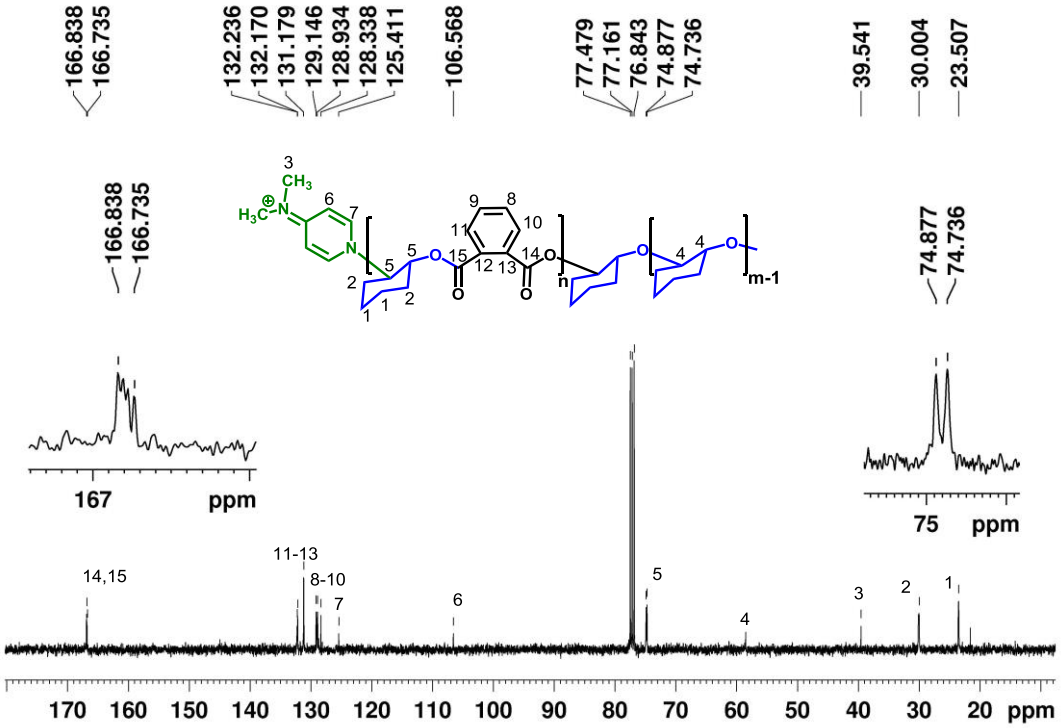

Figure S10. ^{13}C {^{1}H} NMR spectrum ($CDCl_3$, 100 MHz, 298K) of P(PA-*alt*-CHO) copolymer derived by the action of $B(C_2H_5)_3$ and DMAP ($B(C_2H_5)_3$/DMAP/PA/CHO = 2/1/100/100, Table 1 entry 8).

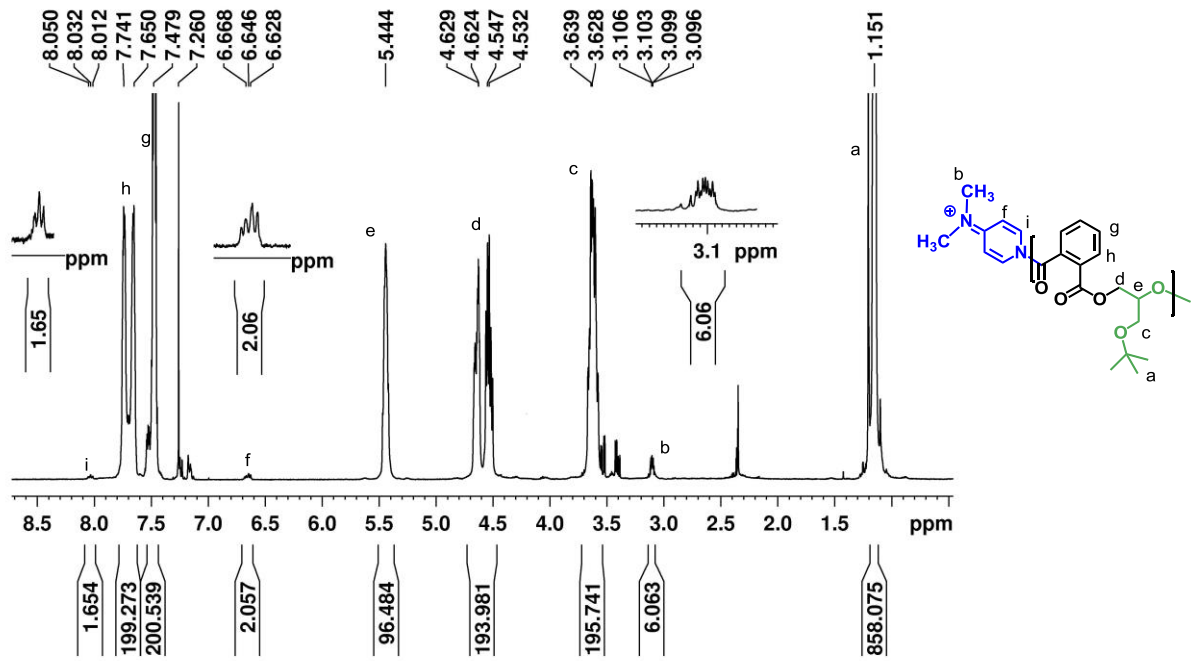

Figure S11. ^{1}H NMR spectrum ($CDCl_3$, 400 MHz, 298K) of P(PA-*alt*-*t*BGE) copolymer derived by the action of $B(C_2H_5)_3$ and DMAP ($B(C_2H_5)_3$/DMAP/PA/*t*BGE = 2/1/100/100, Table 2 entry 12).

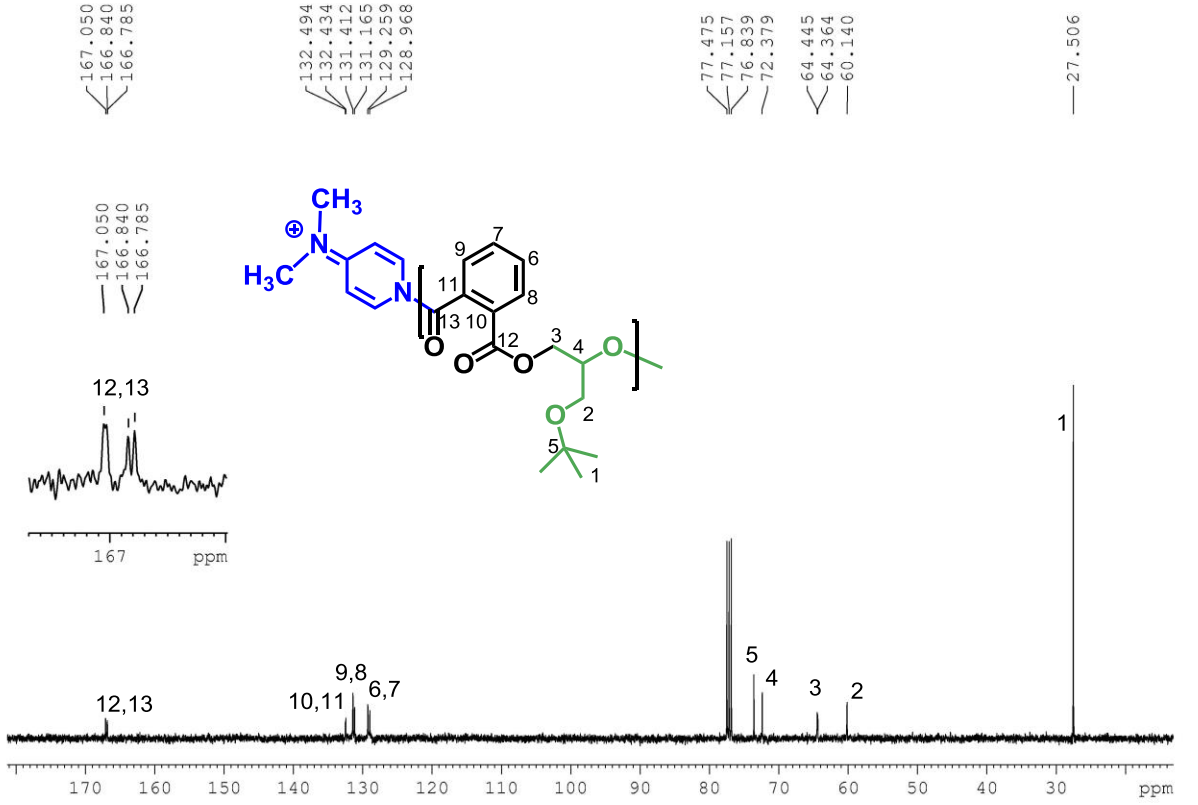

Figure S12. ^{13}C {^{1}H} NMR spectrum ($CDCl_3$, 100 MHz, 298K) of P(PA-*alt*-*t*BGE) copolymer derived by the action of $B(C_2H_5)_3$ and DMAP ($B(C_2H_5)_3$/DMAP/PA/*t*BGE = 2/1/100/100, Table 2 entry 12).

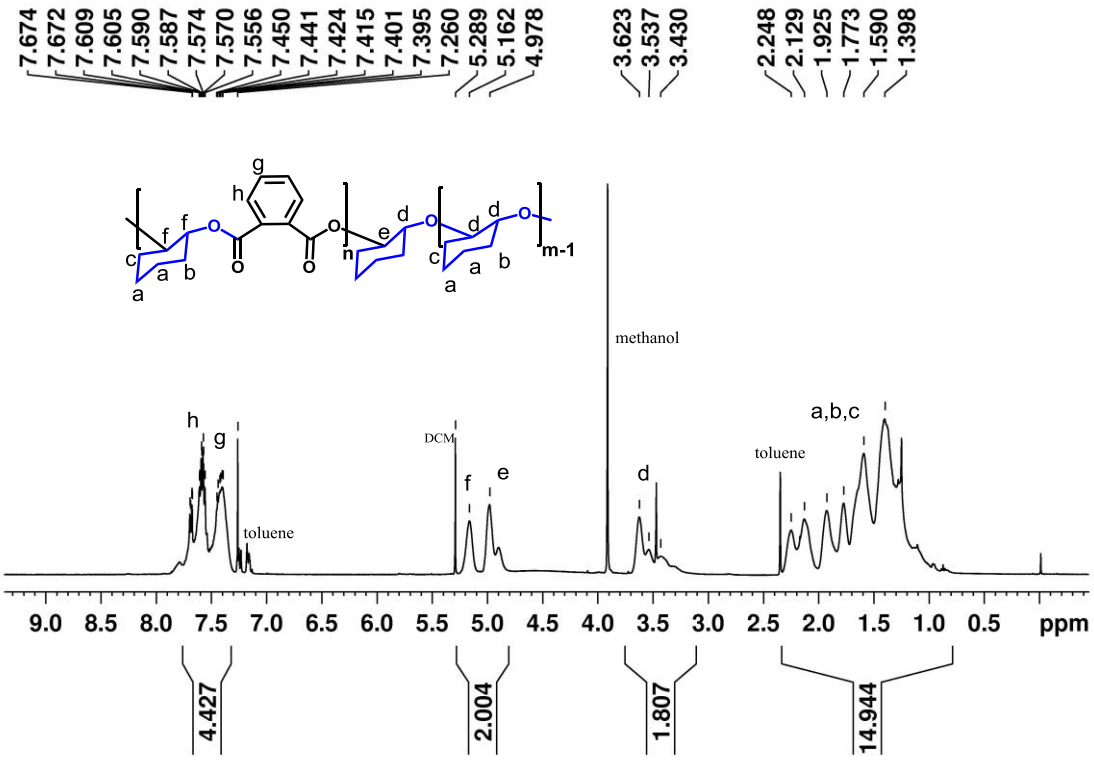

Figure S13. ^{1}H NMR spectrum ($CDCl_3$, 400 MHz, 298K) of P(PA-*alt*-CHO) copolymer derived by the action of $Al(CH)_3$ and PPNCl ($Al(CH)_3$/ PPNCl/PA/CHO = 2/1/200/200, Table 1 entry 13).

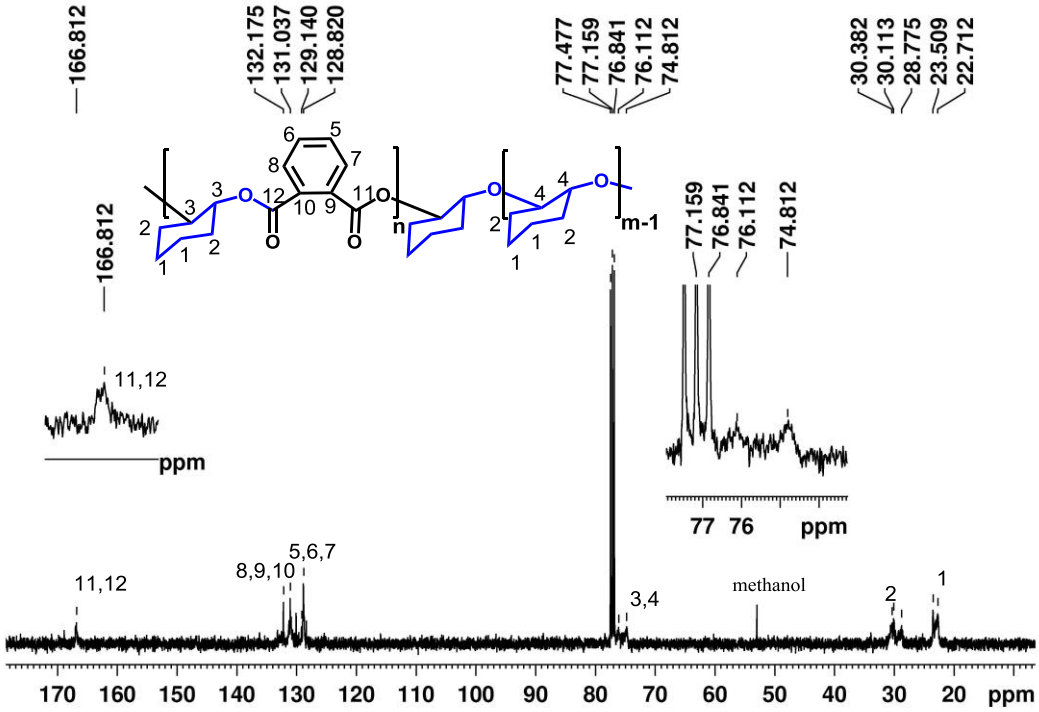

Figure S14. ^{13}C {^{1}H} NMR spectrum ($CDCl_3$, 100 MHz, 298K) of P(PA-*alt*-CHO) copolymer derived by the action of $Al(CH)_3$ and PPNCl ($Al(CH)_3$/ PPNCl/PA/CHO = 2/1/200/200, Table 1 entry 13).

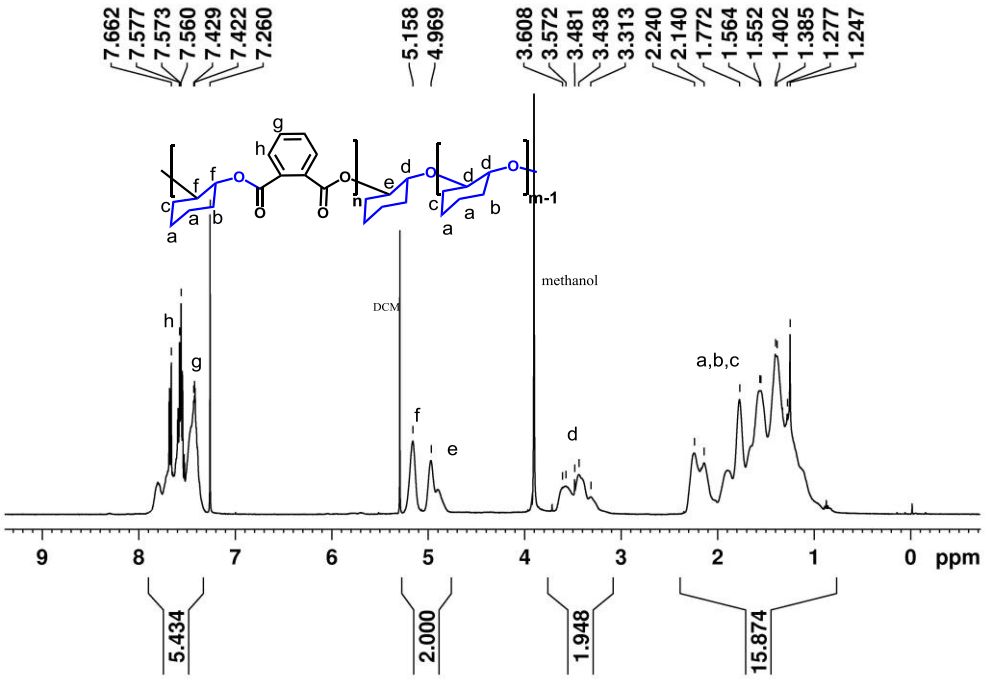

Figure S15. ^{1}H NMR spectrum ($CDCl_3$, 400 MHz, 298K) of P(PA-*alt*-CHO) copolymer derived by the action of Et_2Zn and PPNCl (Et_2Zn/ PPNCl/PA/CHO = 2/1/200/200, Table 1 entry 17).

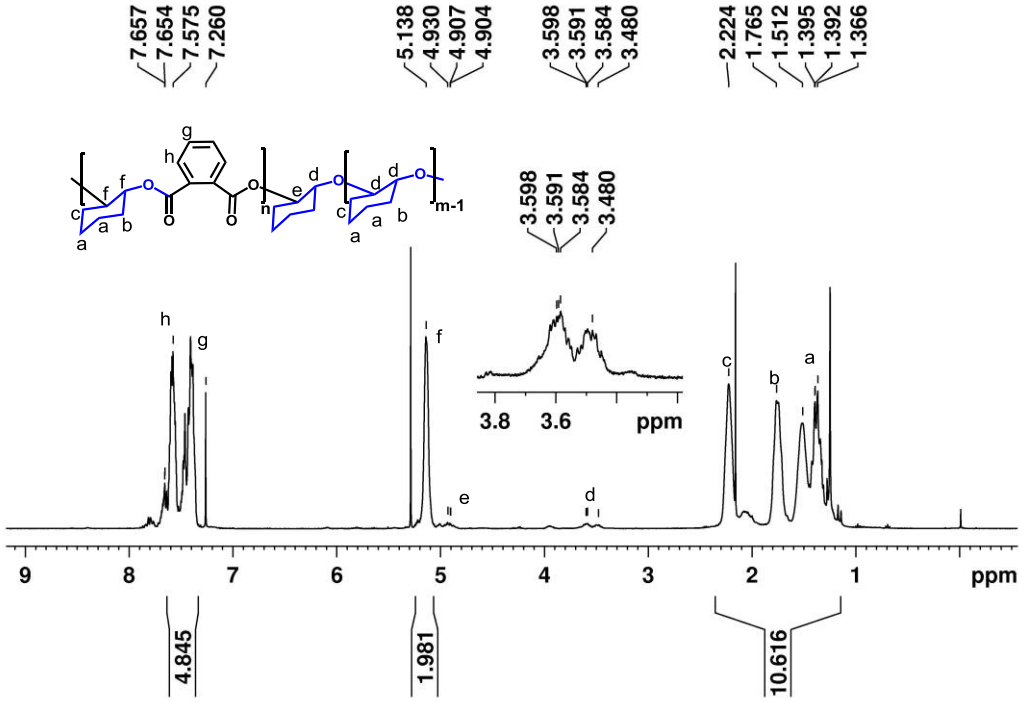

Figure S16. ^{1}H NMR spectrum ($CDCl_3$, 400 MHz, 298K) of P(PA-*alt*-CHO) copolymer derived by the action of $^{n}Bu_2Mg$ and PPNCl ($^{n}Bu_2Mg$/PPNCl/PA/CHO = 2/1/200/200, Table 1 entry 20).

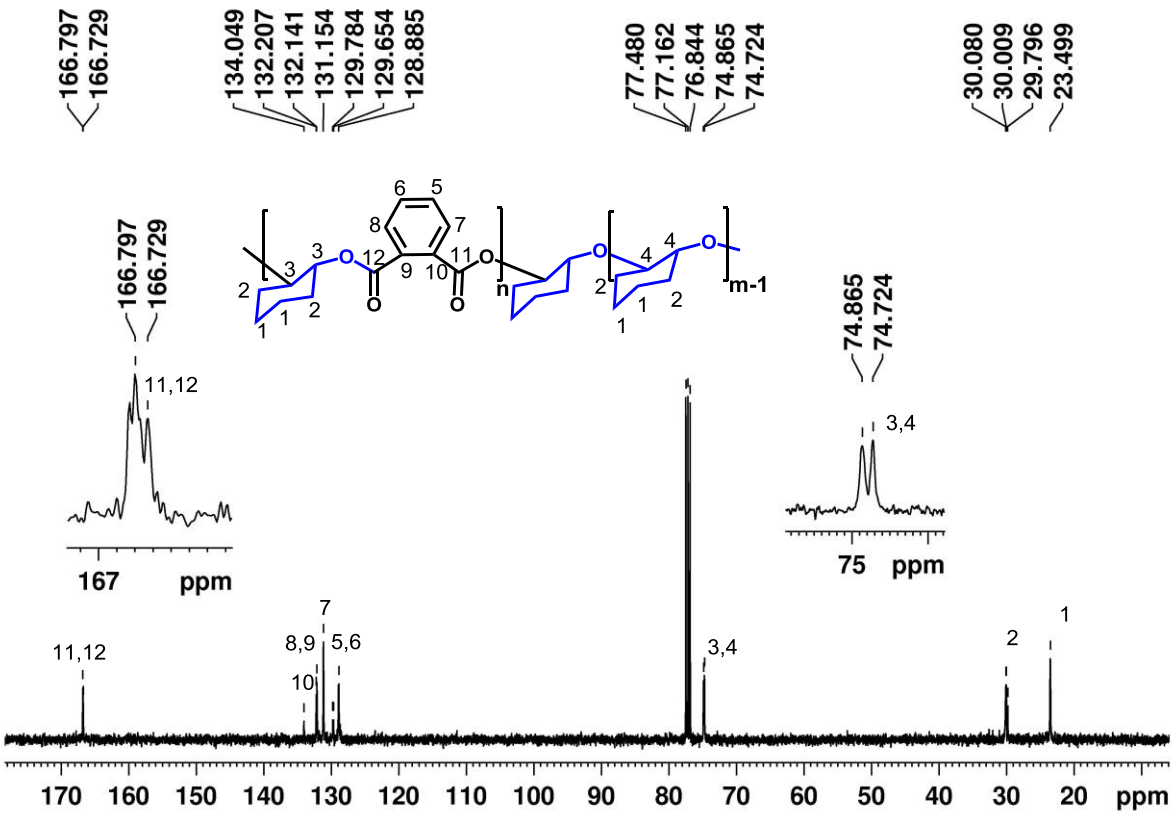

Figure S17. ^{13}C $\{^{1}H\}$ NMR spectrum ($CDCl_3$, 100 MHz, 298K) of P(PA-*alt*-CHO) copolymer derived by the action of $^{n}Bu_2Mg$ and PPNCl ($^{n}Bu_2Mg$/PPNCl/PA/CHO = 2/1/200/200, Table 1 entry 20).

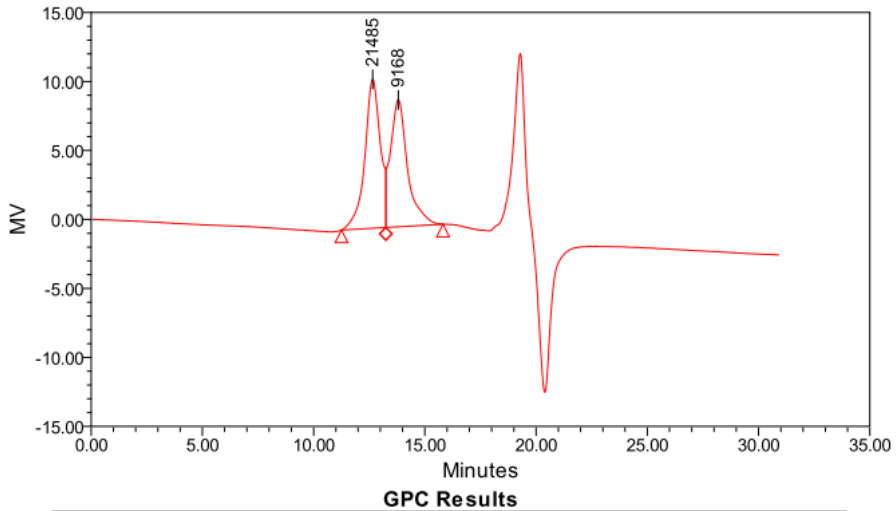

GPC Results

	Dist Name	Name	Retention Time (min)	Injection Volume (uL)	Mn	Mw	MP	Mz	Mz+1	Poly dispersity
1		Peak2	12.655	10.00	21289	22757	21485	24588	26859	1.068951
2		Peak4	13.806	10.00	8034	8852	9168	9526	10085	1.101871

Figure S18. GPC trace of purified product of entry 4 in Table 2.

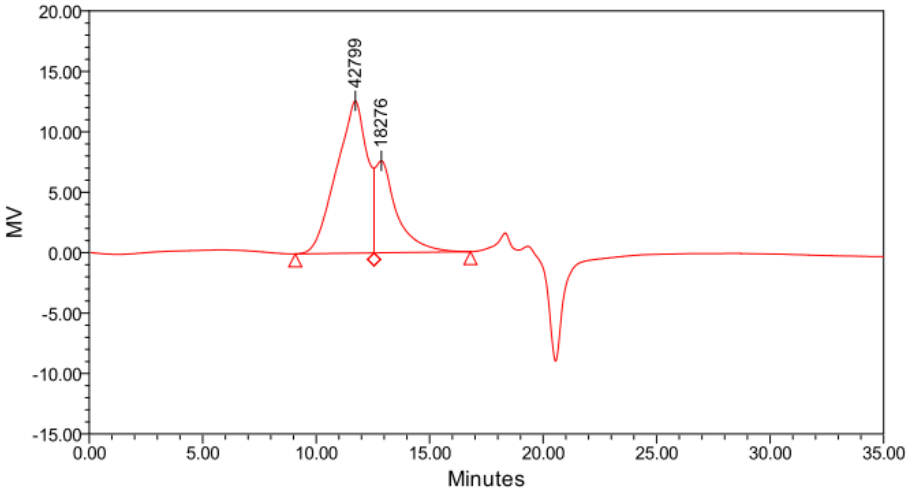

GPC Results

	Dist Name	Name	Retention Time (min)	Injection Volume (uL)	Mn	Mw	MP	Mz	Mz+1	Poly dispersity
1		Peak4	11.723	10.00	46086	57030	42799	72737	92460	1.237479
2		Peak2	12.874	10.00	11859	14656	18276	16525	17763	1.235870

Figure S19. GPC trace of purified product of entry 5 in Table 2.

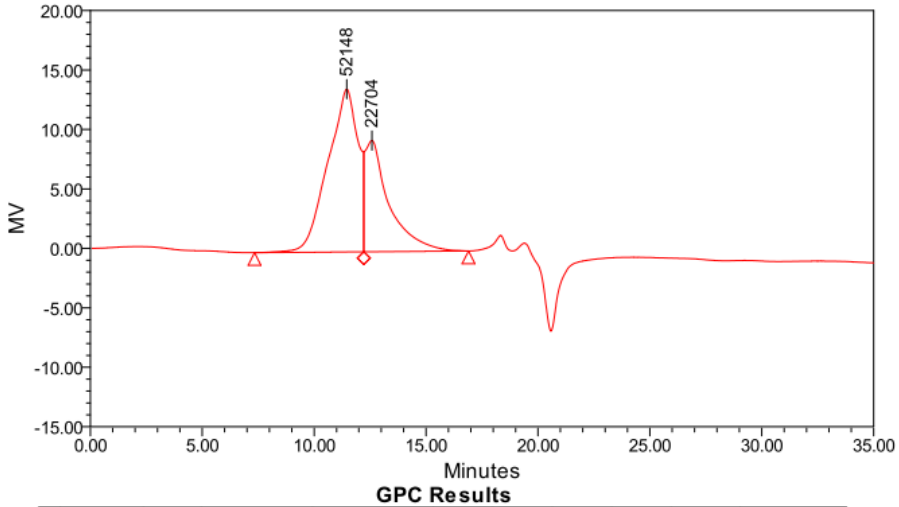

GPC Results

	Dist Name	Name	Retention Time (min)	Injection Volume (uL)	Mn	Mw	MP	Mz	Mz+1	Poly dispersity
1		Peak4	11.456	10.00	57507	71438	52148	92461	120360	1.242258
2		Peak2	12.580	10.00	13216	17595	22704	20514	22363	1.331287

Figure S20. GPC trace of purified product of entry 6 in Table 2.

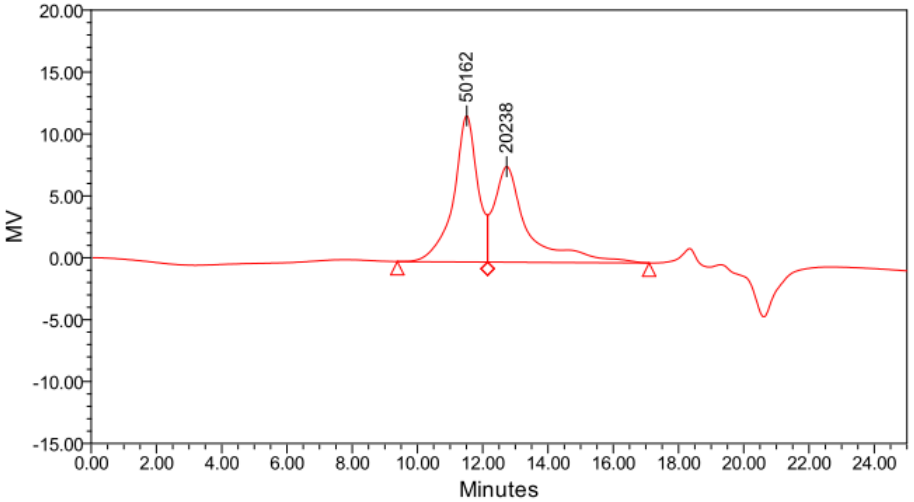

GPC Results

	Dist Name	Name	Retention Time (min)	Injection Volume (uL)	Mn	Mw	MP	Mz	Mz+1	Poly dispersity
1		Peak4	11.508	10.00	51078	55928	50162	62633	71846	1.094957
2		Peak2	12.736	10.00	12260	17231	20238	20346	22238	1.405448

Figure S21. GPC trace of purified product of entry 7 in Table 2.

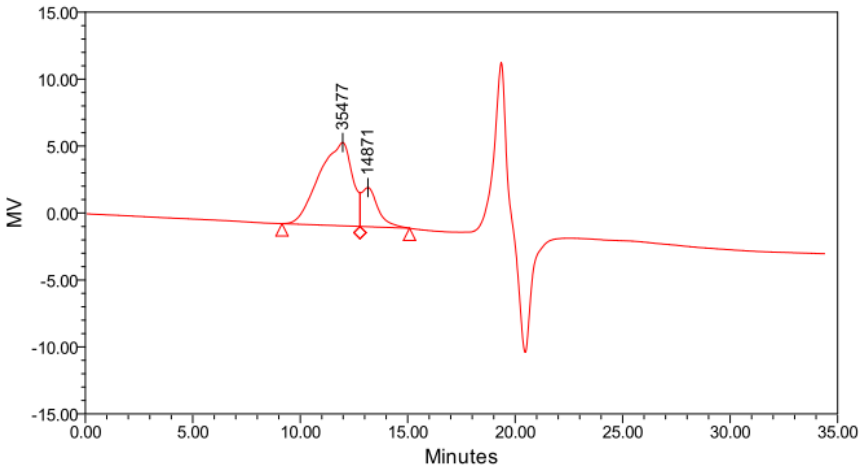

GPC Results

	Dist Name	Name	Retention Time (min)	Injection Volume (uL)	Mn	Mw	MP	Mz	Mz+1	Poly dispersity
1		Peak4	11.977	10.00	43204	55727	35477	73663	95350	1.289863
2		Peak2	13.152	10.00	12382	13563	14871	14485	15209	1.095395

Figure S22. GPC trace of purified product of entry 8 in Table 2.

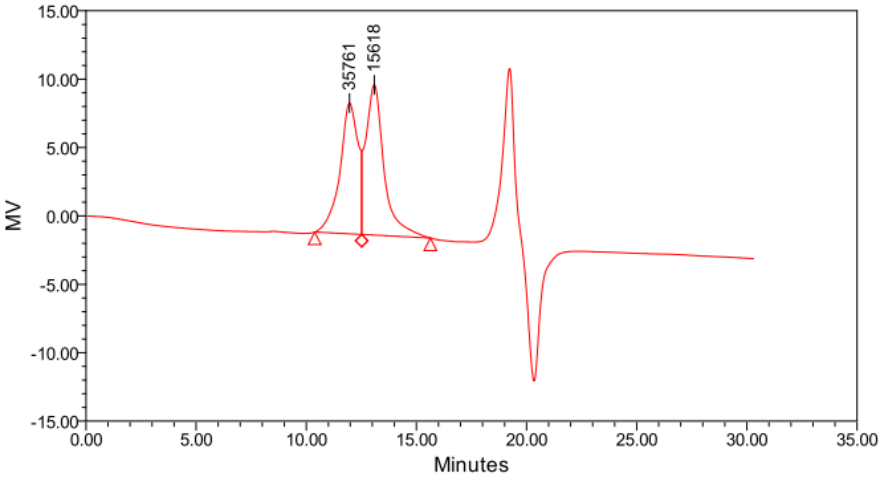

GPC Results

	Dist Name	Name	Retention Time (min)	Injection Volume (uL)	Mn	Mw	MP	Mz	Mz+1	Poly dispersity
1		Peak4	11.966	10.00	36319	39580	35761	43884	49356	1.089789
2		Peak2	13.086	10.00	12990	14975	15618	16378	17439	1.152827

Figure S23. GPC trace of purified product of entry 14 in Table 2.

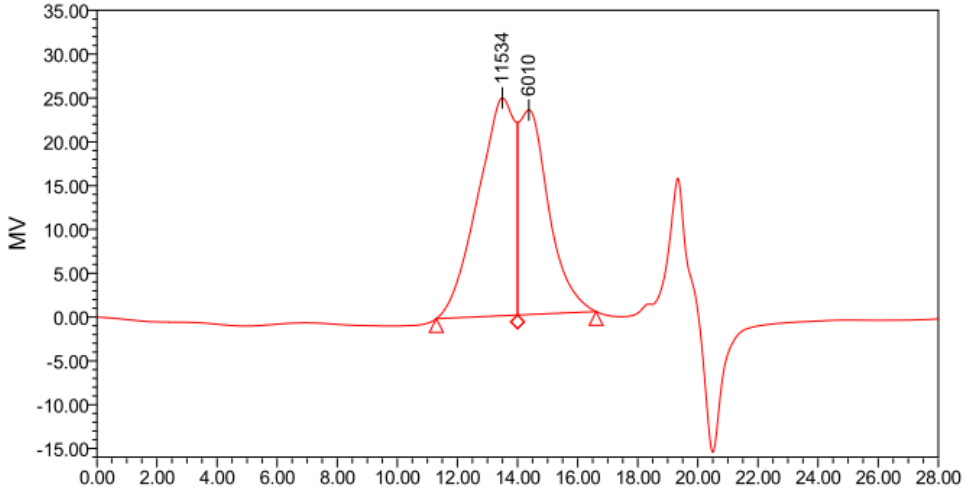

GPC Results

	Dist Name	Name	Retention Time (min)	Injection Volume (uL)	Mn	Mw	MP	Mz	Mz+1	Poly dispersity
1		Peak2	13.496	10.00	13551	16049	11534	19636	24119	1.184335
2		Peak4	14.378	10.00	4825	5280	6010	5692	6042	1.094369

Figure S24. GPC trace of purified product of entry 7 in Table 1.

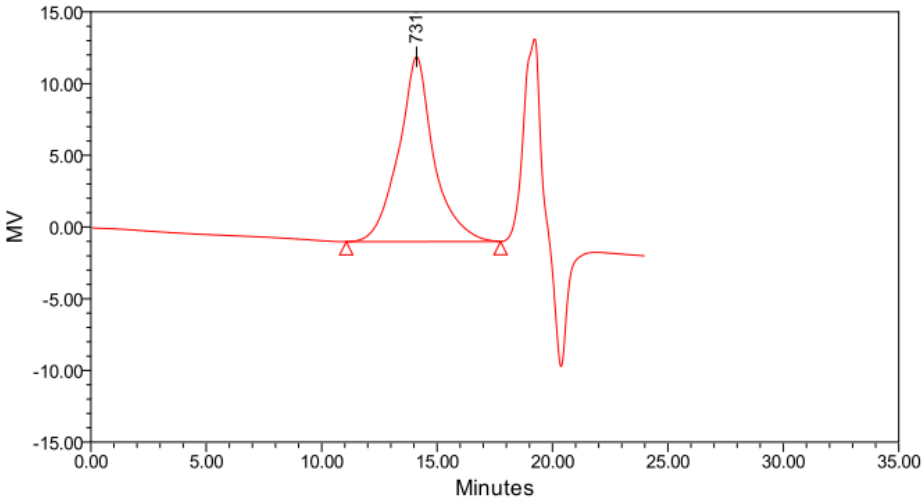

GPC Results

	Dist Name	Name	Retention Time (min)	Injection Volume (uL)	Mn	Mw	MP	Mz	Mz+1	Poly dispersity
1		Peak4	14.112	10.00	6774	9101	7316	12686	17836	1.343531

Figure S25. GPC trace of purified product of entry 13 in Table 1.

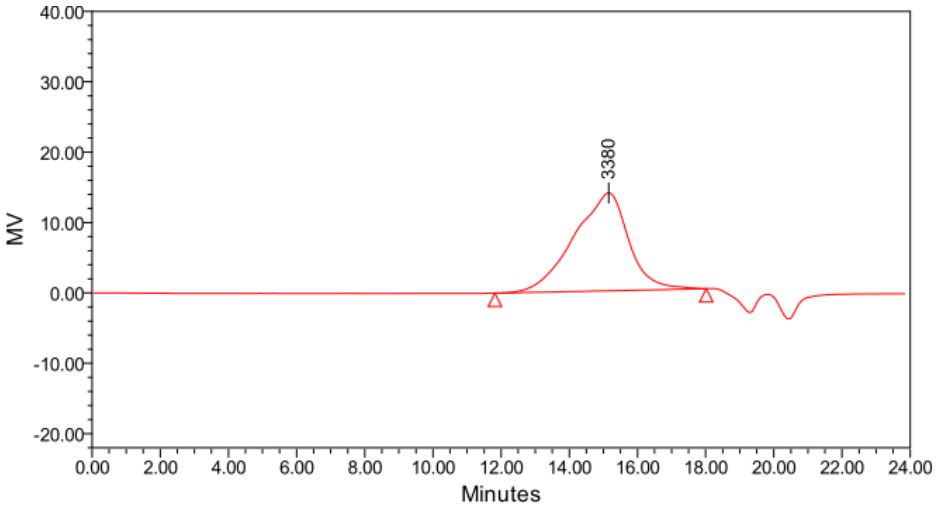

GPC Results

	Dist Name	Name	Retention Time (min)	Injection Volume (uL)	Mn	Mw	MP	Mz	Mz+1	Poly dispersity
1		Peak4	15.156	10.00	4413	5589	3380	7558	10403	1.266484

Figure S26. GPC trace of purified product of entry 20 in Table 1.

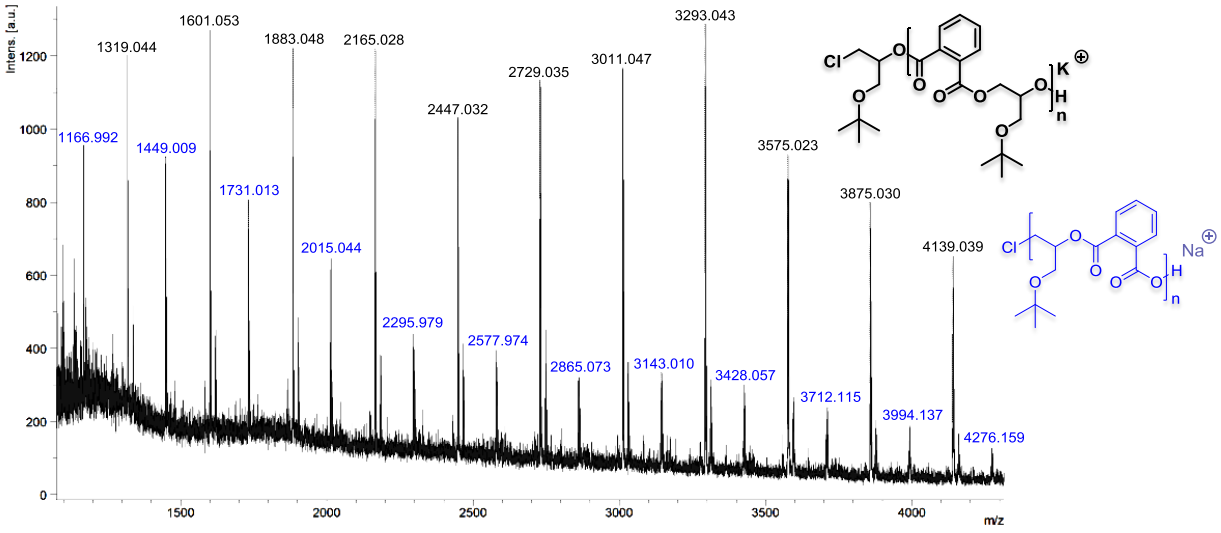

Figure S27. MALDI-TOF MS spectrum of the low-molecular-weight P(PA-*alt*-*t*BGE) polyester synthesized by the catalysis of TEB/PPNCl-based LP. The two (**black** and **blue**) series shows m/z = [35.45 (Cl) +130.19 (*t*BGE) + (278.31 × n) (PA+ *t*BGE) + 39.1 (K^+) + 1.01 (H^+)] (n = 4~14) for **black**; m/z = [35.45 (Cl) + (278.31 × n) (PA+ *t*BGE) + 22.99 (Na^+) + 1.01 (H^+)] (n = 4~15) for **blue**.

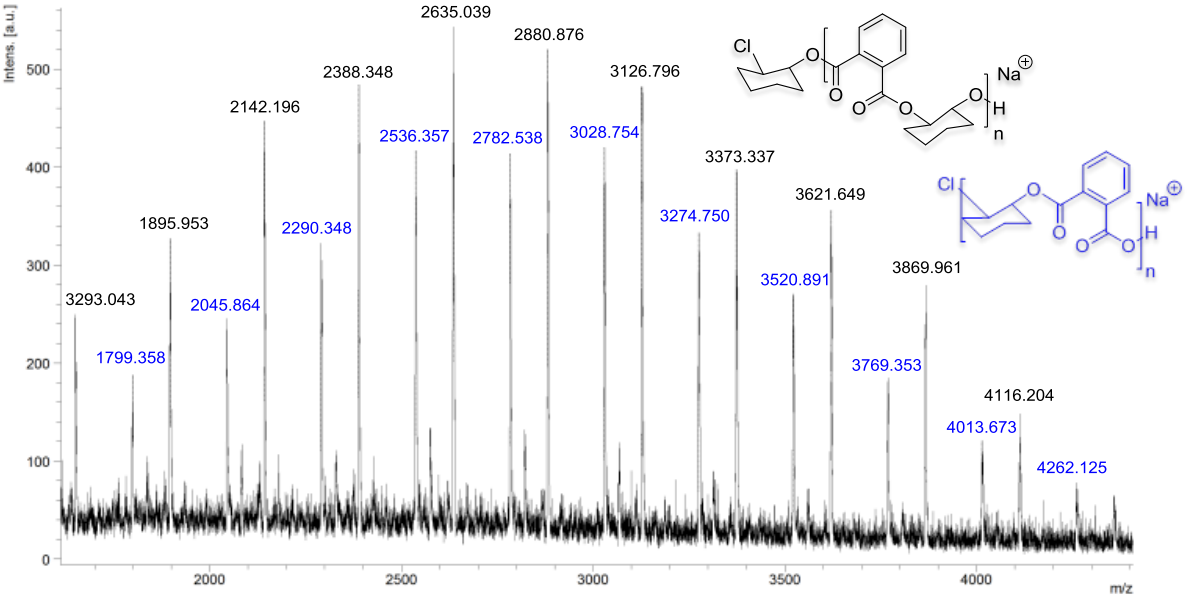

Figure S28. MALDI-TOF MS spectrum of the low-molecular-weight P(PA-*alt*-CHO) polyester synthesized by the catalysis of TEB/PPNCl-based LP. The two (**black** and **blue**) series shows m/z = [35.45 (Cl) +98.15 (CHO) + (246.27×n) (PA+CHO) + 22.99 (Na^+) + 1.01 (H^+)] (n = 6~16) for **black**; m/z = [35.45 (Cl) + (246.27× n) (PA+ CHO) + 22.99 (Na^+) + 1.01 (H^+)] (n = 7~17) for **blue**.

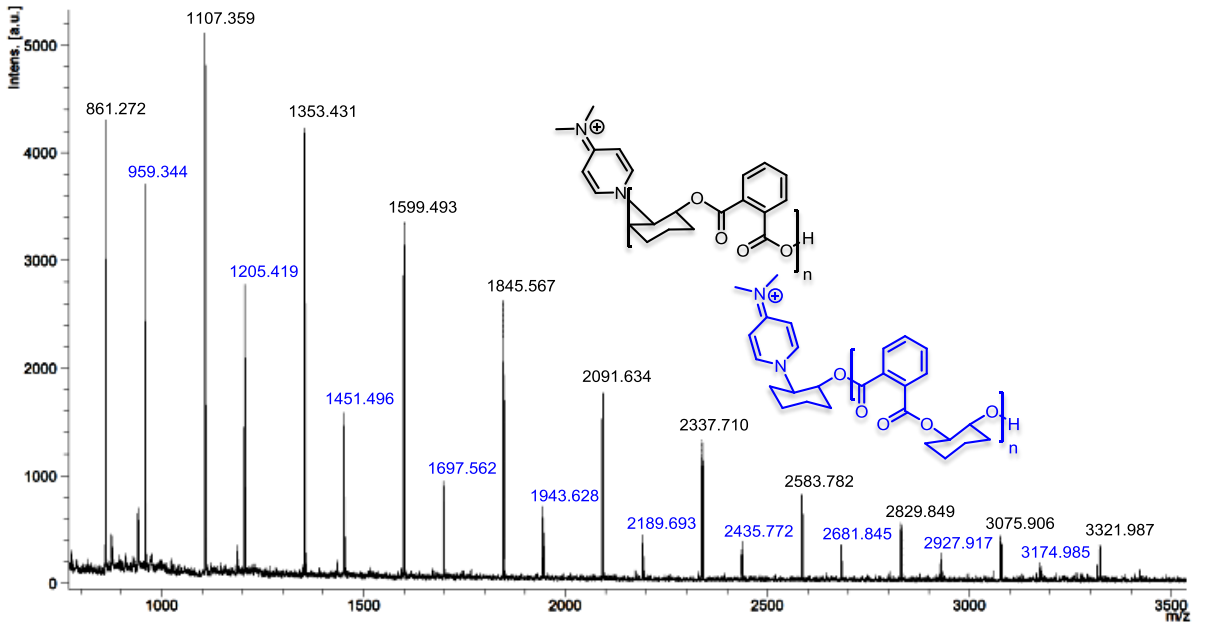

Figure S29. MALDI-TOF MS spectrum of the low-molecular-weight P(PA-*alt*-CHO) polyester synthesized by the catalysis of TEB/DMAP-based LP. The two (**black** and **blue**) series shows m/z = [122.17 (DMAP) + (246.27×n) (PA+CHO) + 1.01 (H^+)] (n = 3~13) for **black**; m/z = [122.17 (DMAP) +98.15 (CHO) + (246.27×n) (PA+CHO) + 1.01 (H^+)] (n = 3~12) for **blue**.

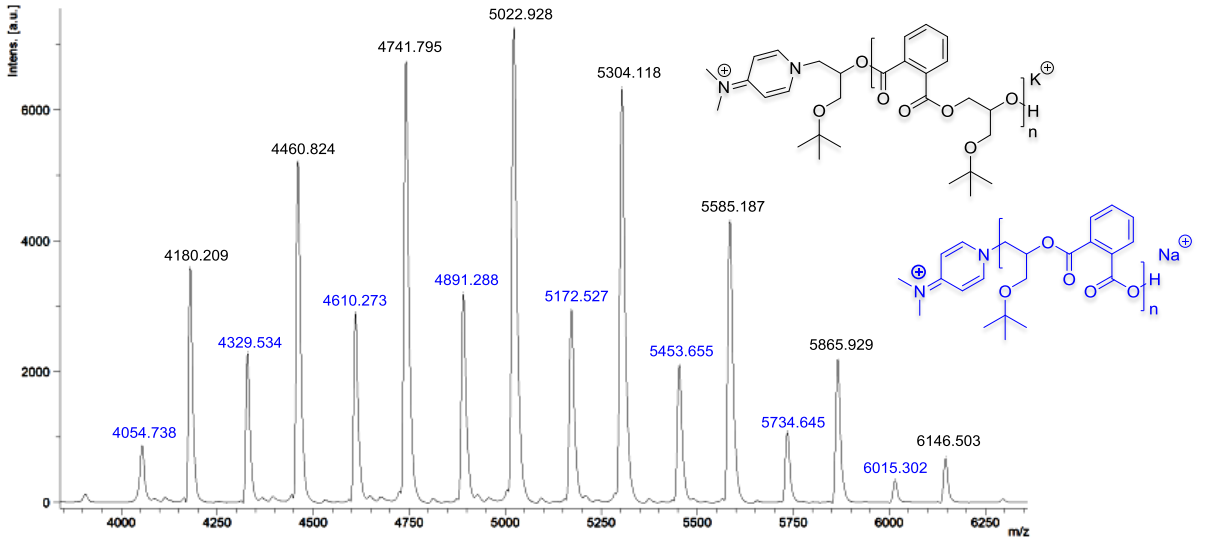

Figure S30. MALDI-TOF MS spectrum of the low-molecular-weight P(PA-*alt*-*t*BGE) polyester synthesized by the catalysis of TEB/DMAP-based LP. The two (**black** and **blue**) series shows m/z = [122.17 (DMAP) + 130.19 (*t*BGE) + (278.31 × n) (PA+ *t*BGE) + 39.1 (K^+) + 1.01 (H^+)] (n = 14~21) for **black**; m/z = [122.17 (DMAP) + (278.31 × n) (PA+ *t*BGE) + 22.99 (Na^+) + 1.01 (H^+)] (n = 14~21) for **blue**.

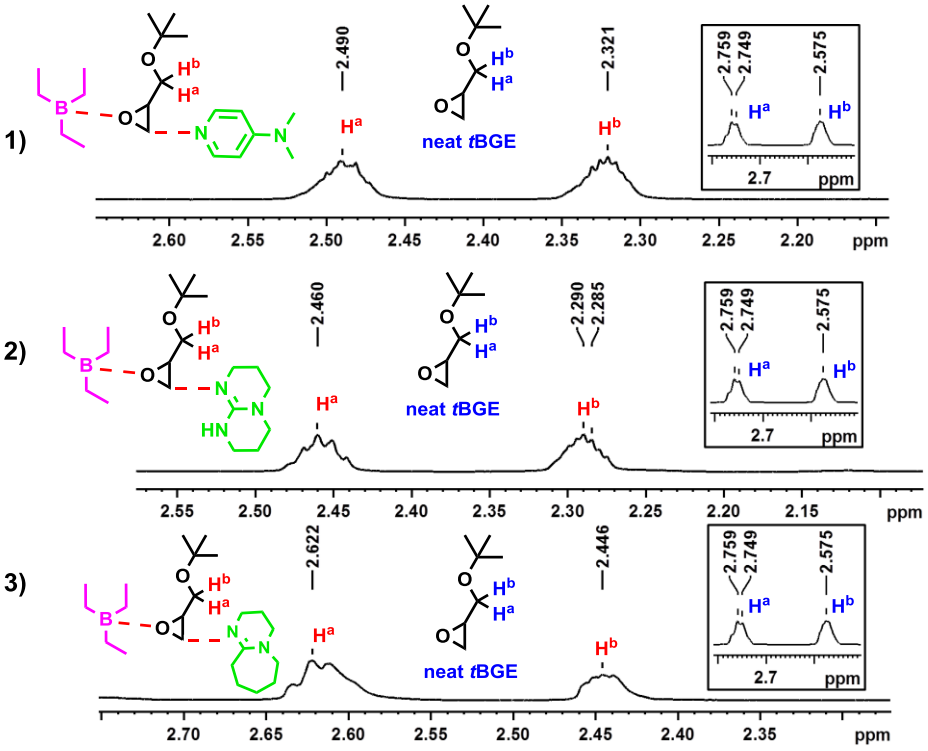

Figure S31. (1) ^{1}H NMR ($CDCl_3$, 400 MHz, 298K) spectra of *t*BGE activation by TEB/DMAP pair; (2) ^{1}H NMR spectra of *t*BGE activation by TEB/TBD pair; (3) ^{1}H NMR spectra of *t*BGE activation by TEB/DBU pair; (Inset figure shows the chemical shifts of the H^a and H^b signals of neat *t*BGE (2.75 and 2.57 ppm).

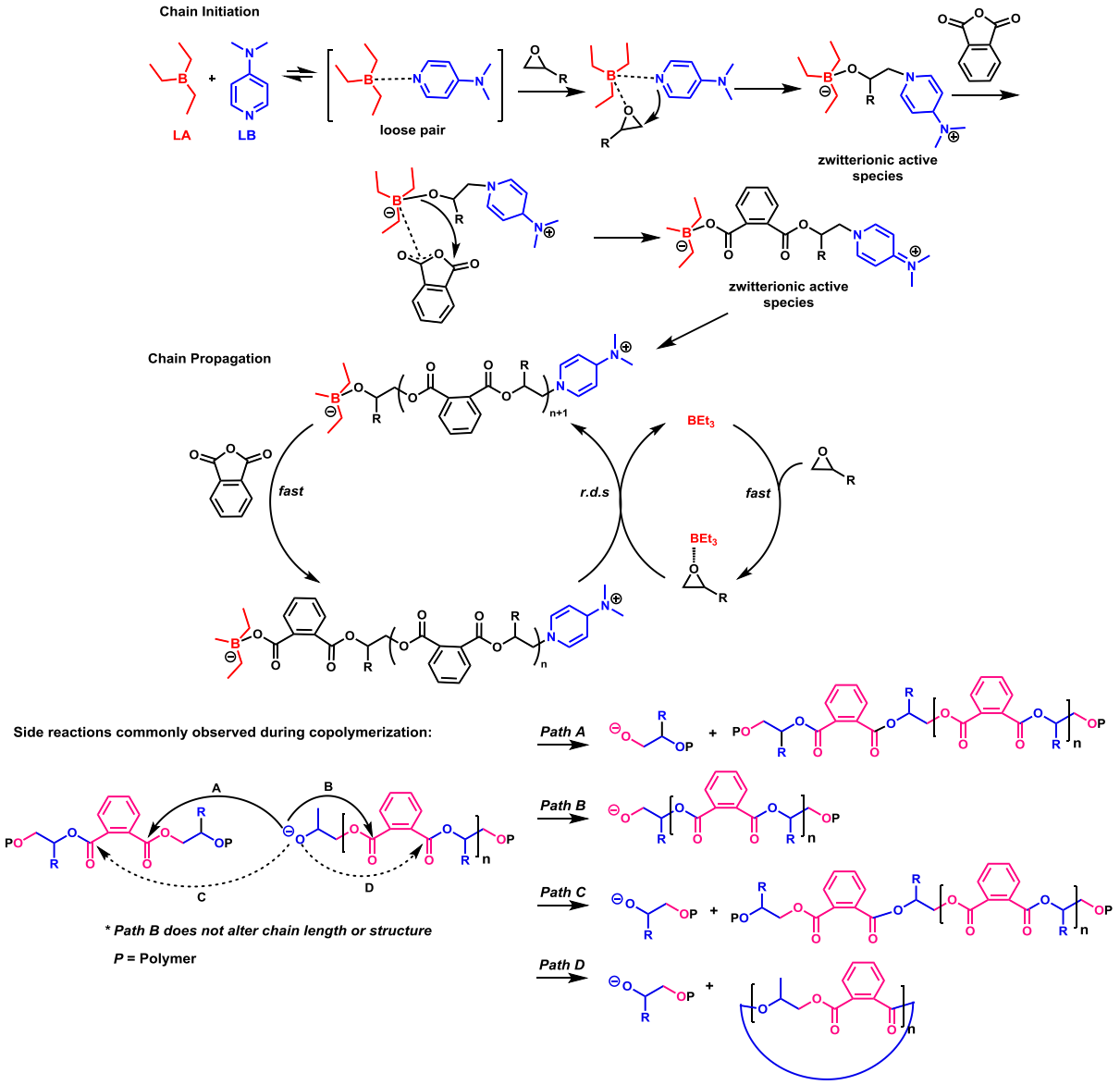

Figure S32. Proposed cooperative mechanism for the zwitter ionic copolymerization of epoxides and PA catalyzed by $B(C_2H_5)_3$/DMAP-based Lewis pair.

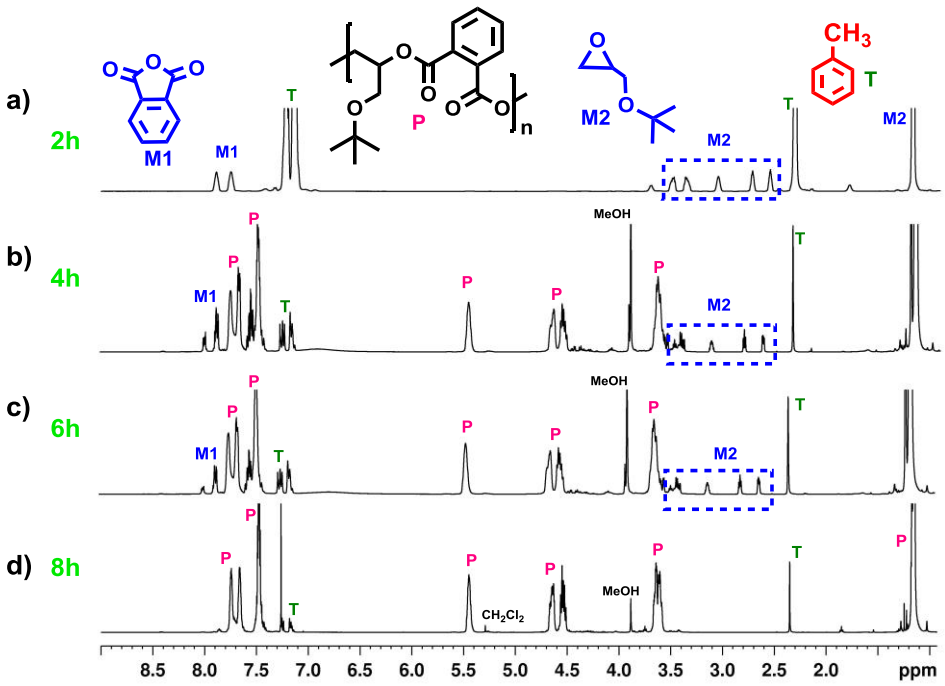

Figure S33. Overlap of ^{1}H NMR monitoring of copolymerization of *t*BGE and PA catalyzed by $B(C_2H_5)_3$/PPNCl-based Lewis pair ($B(C_2H_5)_3$/PPNCl/PA/*t*BGE = 2/1/200/200, Table 2 entry 8).

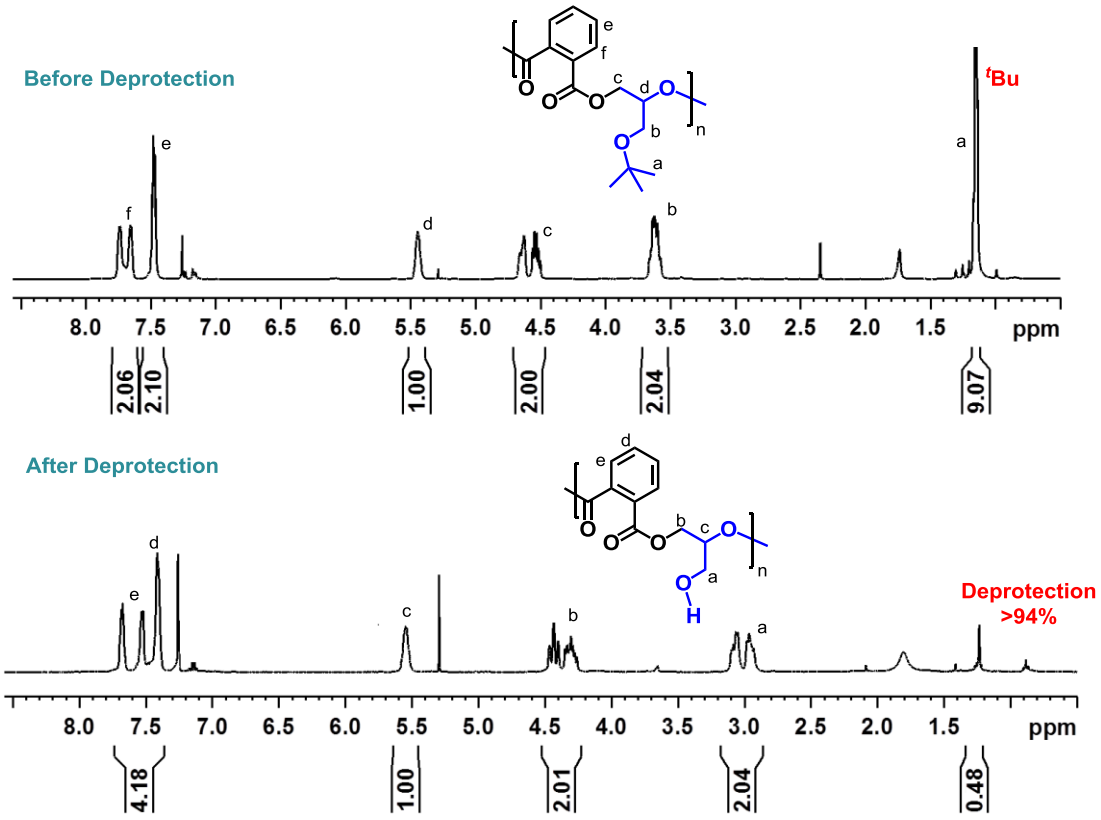

Figure S34. ^{1}H NMR spectra ($CDCl_3$, 400 MHz, 298K) of P(PA-*alt*- *t*BGE)copolymer before and after deprotection of ^{t}Bu groups.

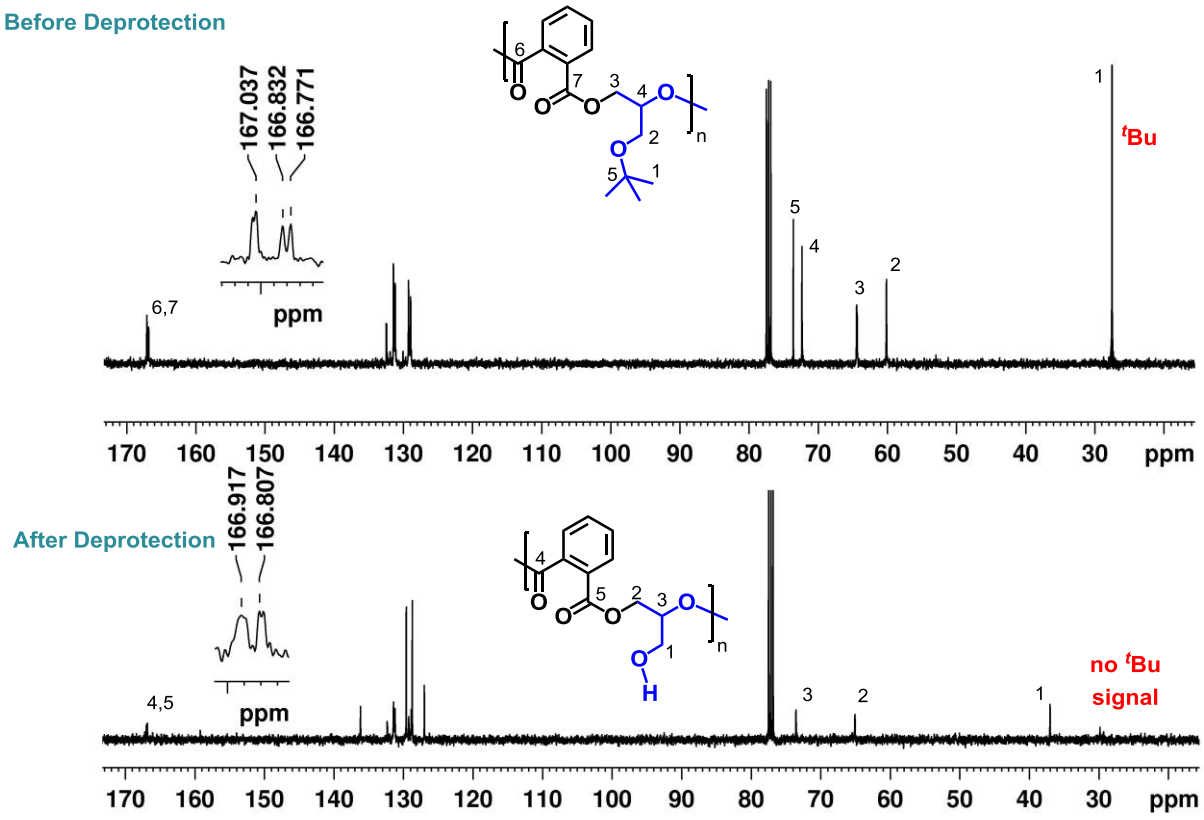

Figure S35. Representative ^{13}C NMR spectra ($CDCl_3$, 100 MHz, 298K) of P(PA-*alt*-*t*BGE) copolymer before and after deprotection of ^{t}Bu groups.

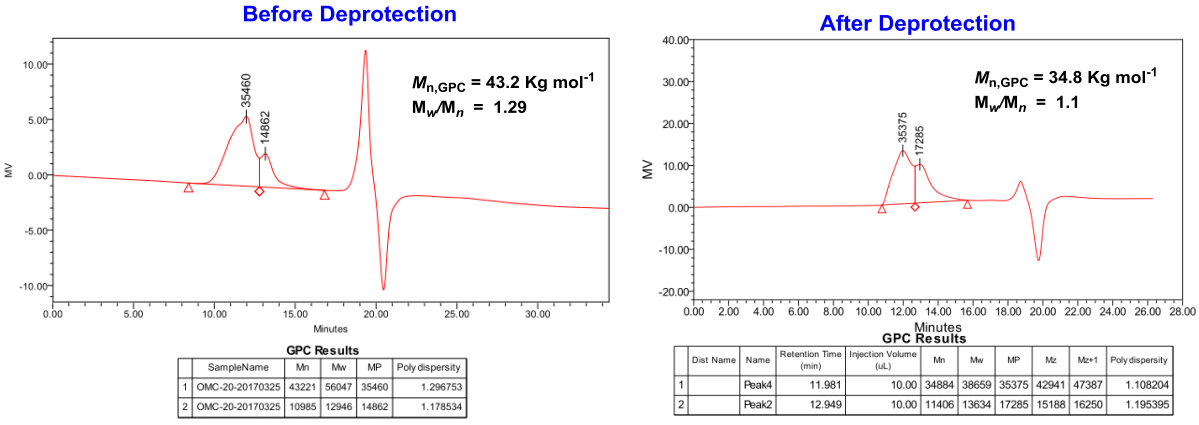

Figure S36. GPC curves of purified products before and after deprotection.

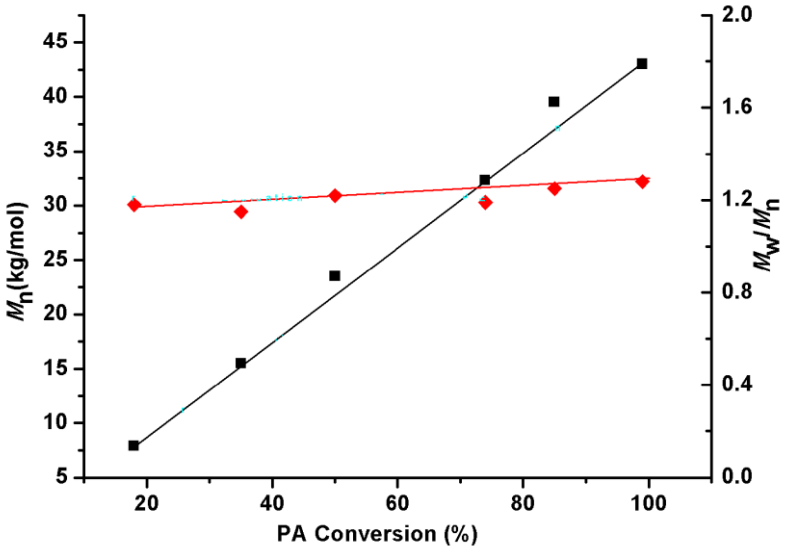

Figure S37. Plot of M_n and M_w/M_n *vs.* PA conversion using Et_3B and PPNCl as catalyst at initiator/monomers ratio, Et_3B/ PPNCl/PA/*t*BGE = 2/1/200/200.

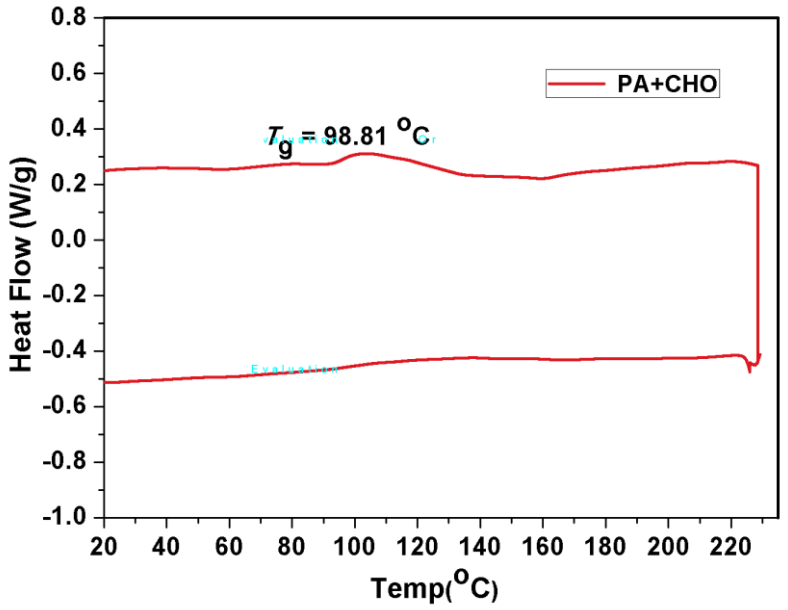

Figure S38. DSC trace (heating rate: 10 °C/min, 2nd scan) of P(PA-*alt*-CHO) copolymer derived by the action of Et_3B and PPNCl (Et_3B/ PPNCl/PA/CHO = 2/1/200/200, Table 2 entry 4).

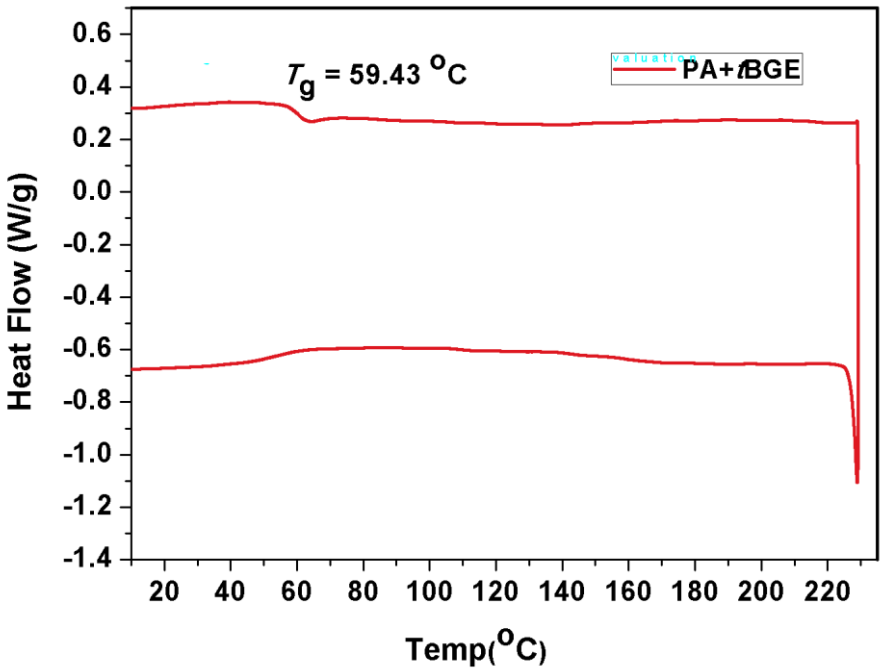

Figure S39. DSC trace (heating rate: 10 °C/min, 2nd scan) of P(PA-*alt*-*t*BGE) copolymer derived by the action of Et_3B and PPNCl (Et_3B/ PPNCl/PA/*t*BGE = 2/1/200/200, Table 2 entry 8).

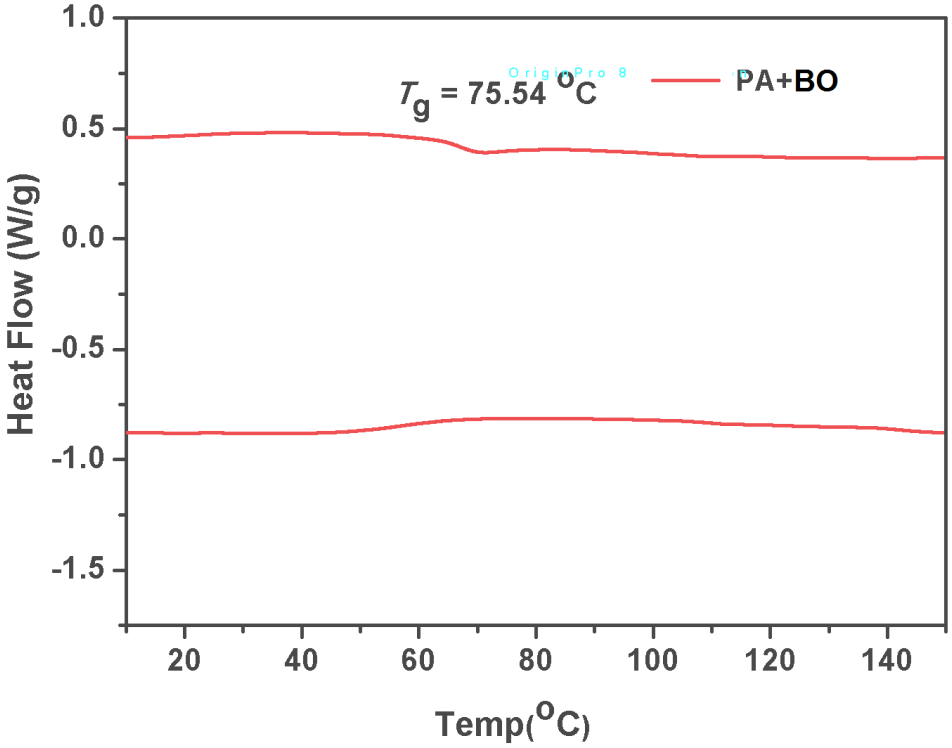

Figure S40. DSC trace (heating rate: 10 °C/min, 2nd scan) of P(PA-*alt*-BO) copolymer derived by the action of Et_3B and PPNCl (Et_3B/ PPNCl/PA/BO = 2/1/200/200, Table 2 entry 14).

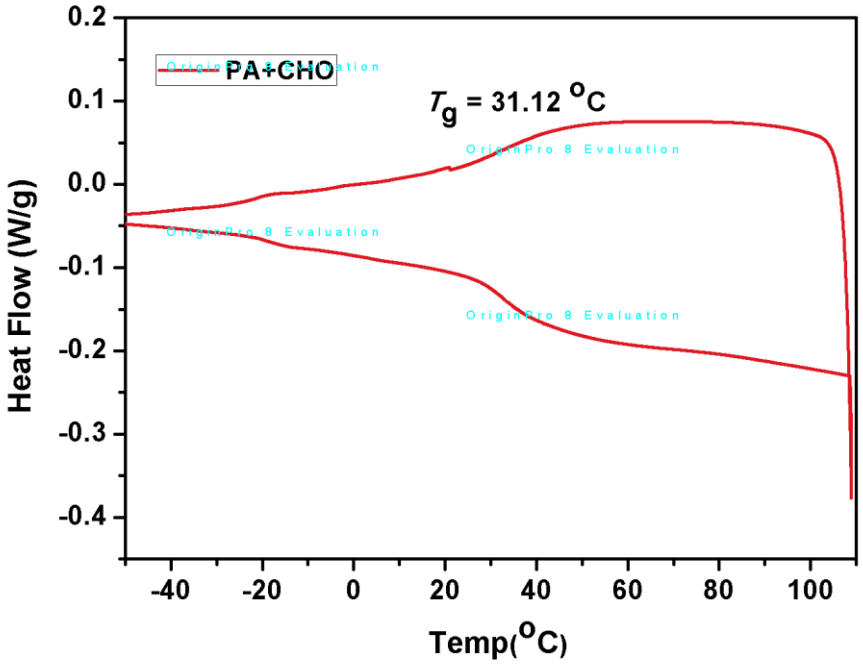

Figure S41. DSC trace (heating rate: 10 °C/min, 2nd scan) of P(PA-*alt*-CHO) copolymer derived by the action of $Al(CH)_3$ and PPNCl ($Al(CH)_3$/PPNCl/PA/CHO = 2/1/200/200, Table 1 entry 13).

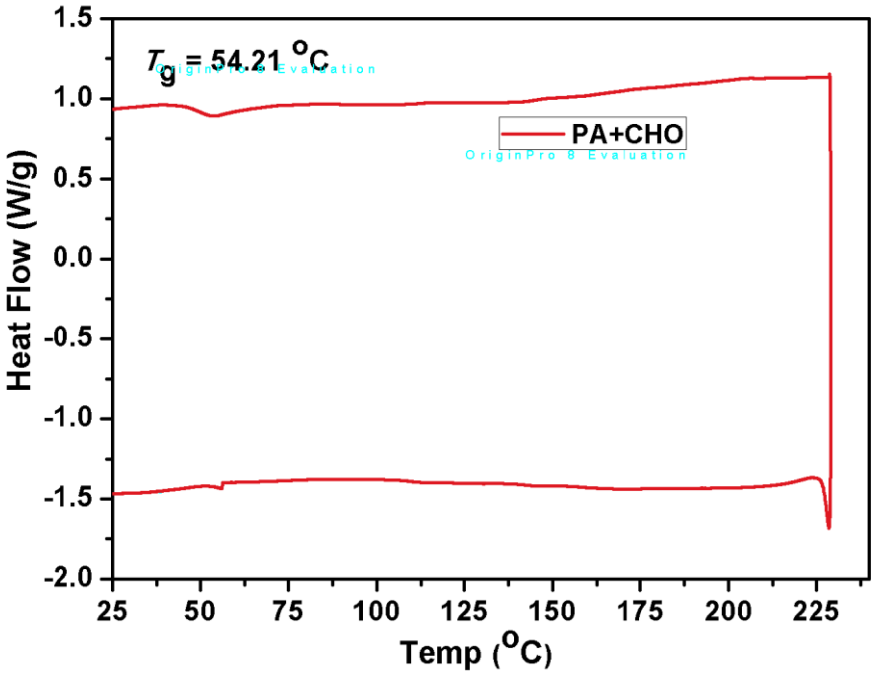

Figure S42. DSC trace (heating rate: 10 °C/min, 2nd scan) of P(PA-*alt*-CHO) copolymer derived by the action of $^nBu_2Mg$ and PPNCl ($^nBu_2Mg$/PPNCl/PA/CHO = 2/1/200/200, Table 1 entry 20).

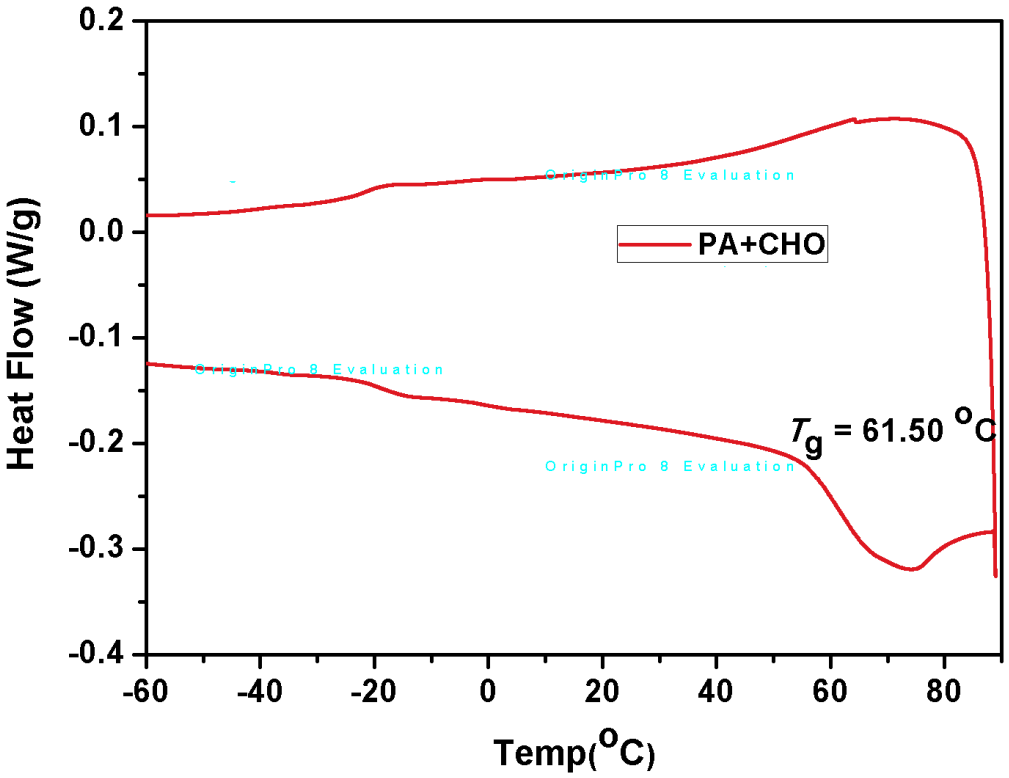

Figure S43. DSC trace (heating rate: 10 °C/min, 2nd scan) of P(PA-*alt*-CHO) copolymer derived by the action of Et_3B and DMAP (Et_3B / DMAP/PA/CHO = 2/1/200/200, Table 1 entry 7).

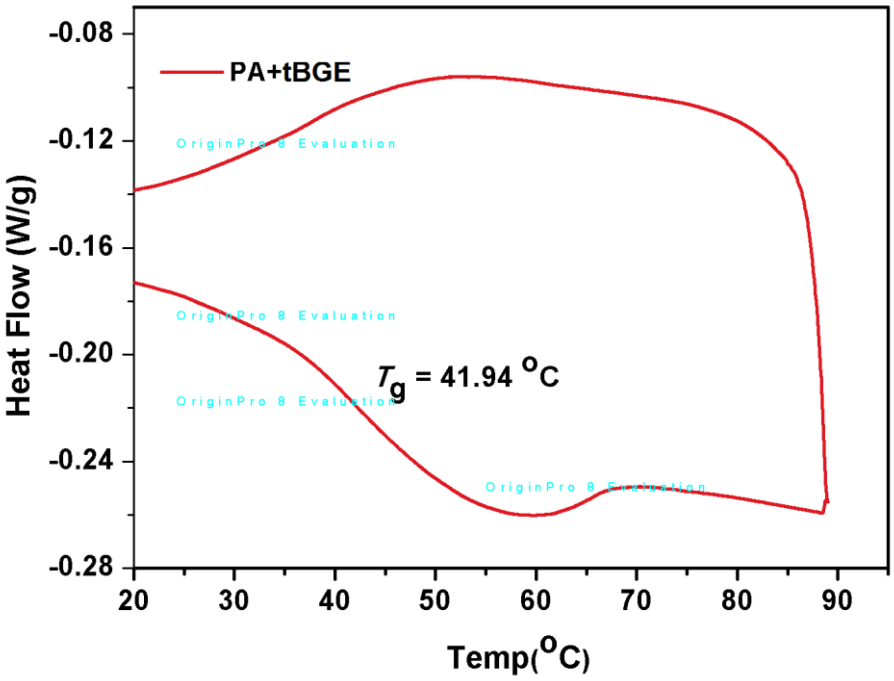

Figure S44. DSC trace (heating rate: 10 °C/min, 2nd scan) of P(PA-*alt*-*t*BGE) copolymer derived by the action of Et_3B and DMAP (Et_3B / DMAP/PA/*t*BGE = 2/1/200/200, Table 2 entry 11).

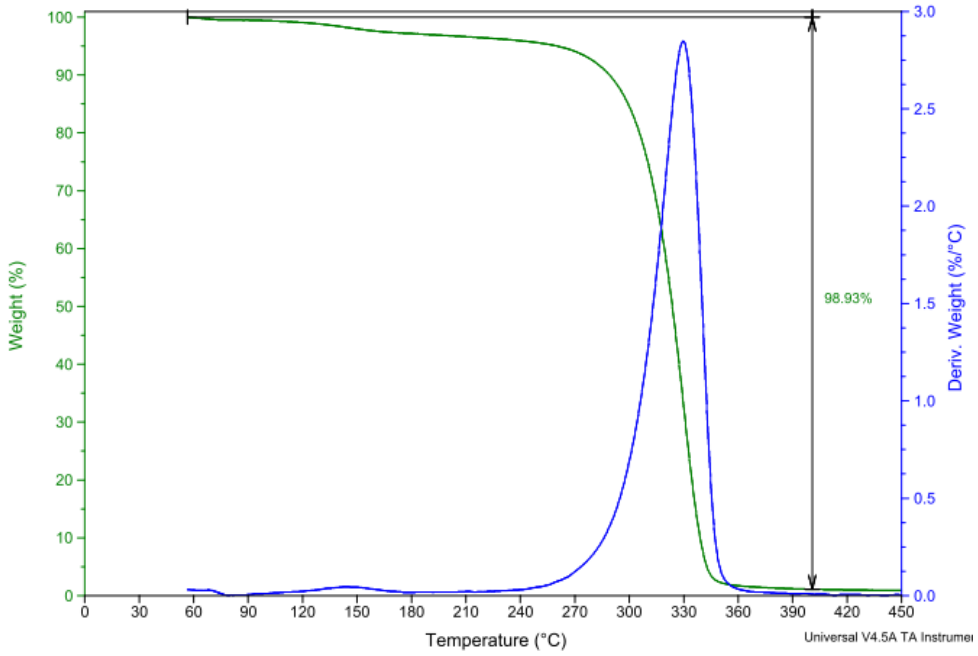

Figure S45. TGA and derivative thermogravimetry (DTG) curves of P(PA-*alt*-CHO) copolymer derived by the action of Et_3B and PPNCl (Et_3B/ PPNCl/PA/CHO = 2/1/200/200, Table 2 entry 4).

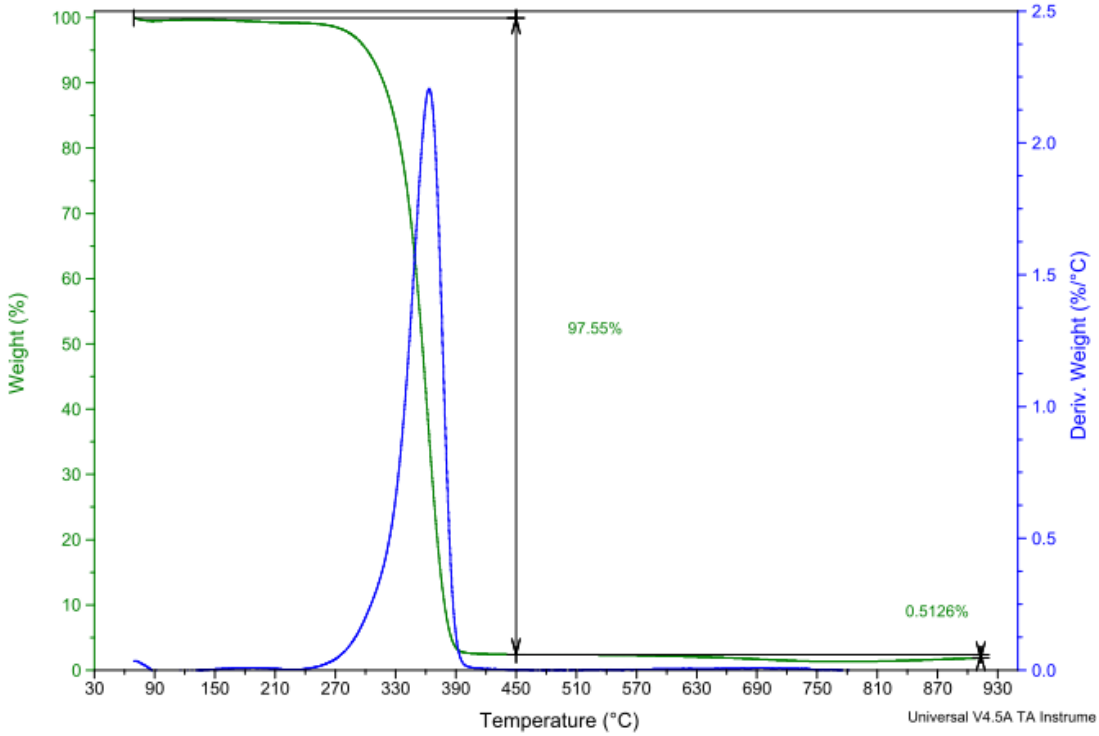

Figure S46. TGA and DTG curves of P(PA-*alt*-*t*BGE) copolymer derived by the action of Et_3B and PPNCl (Et_3B/ PPNCl/PA/*t*BGE = 2/1/200/200, Table 2 entry 8).

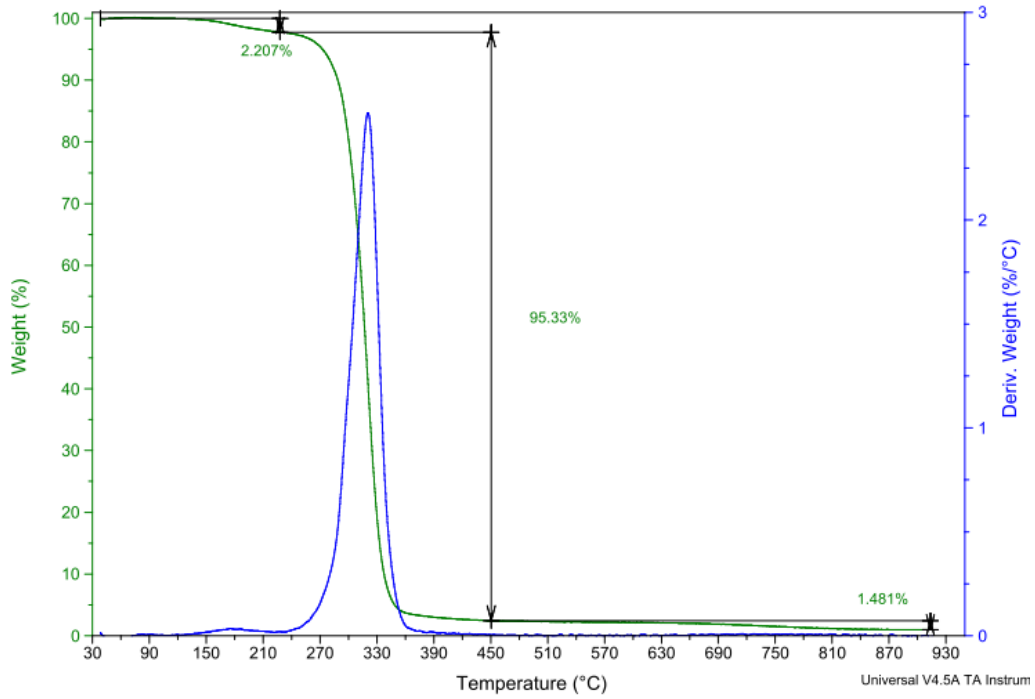

Figure S47. TGA and DTG curves of P(PA-*alt*-BO) copolymer derived by the action of Et_3B and PPNCl (Et_3B/ PPNCl/PA/BO = 2/1/200/200, Table 2 entry 14).

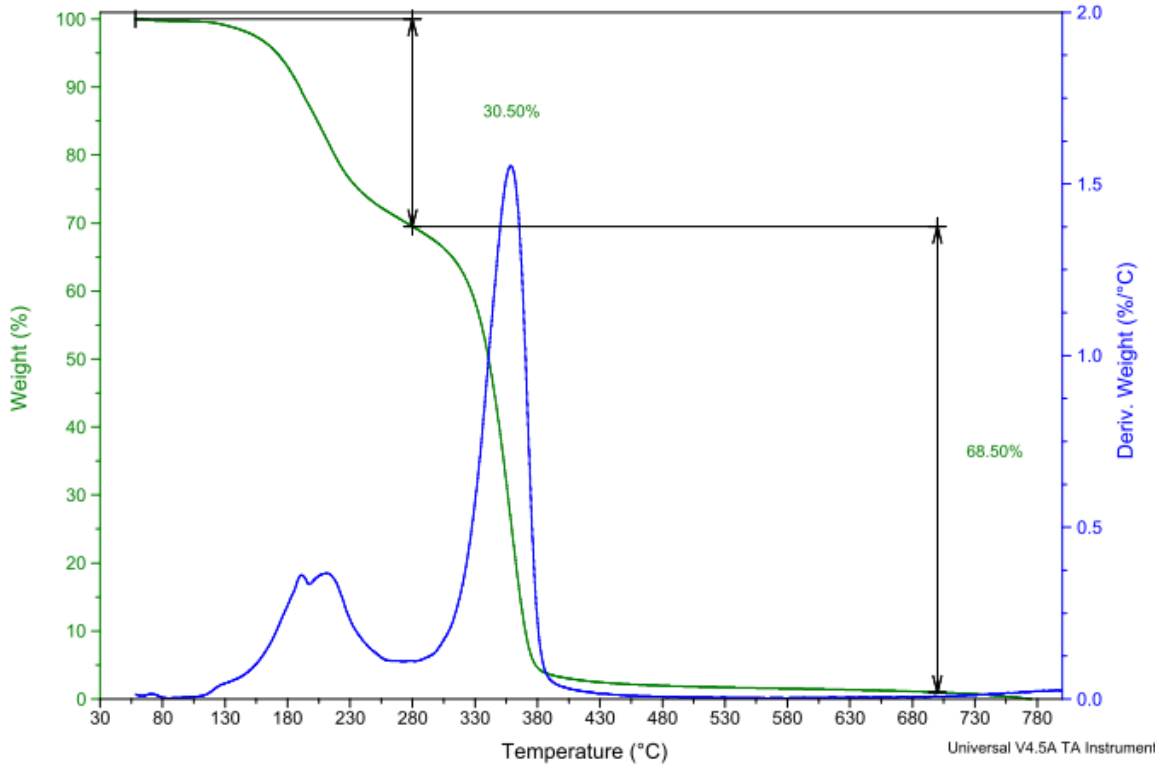

Figure S48. TGA and DTG curves of P(PA-*alt*-CHO) copolymer derived by the action of $Al(CH)_3$ and PPNCl ($Al(CH)_3$/PPNCl/PA/CHO = 2/1/200/200, Table 1 entry 13).

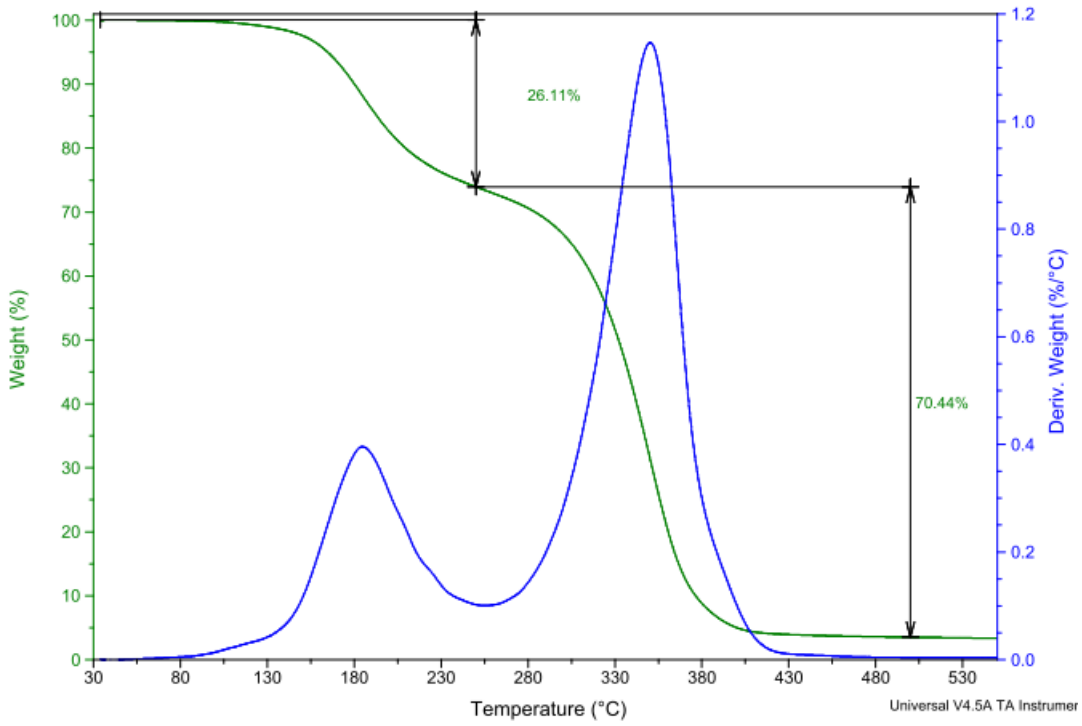

Figure S49. TGA and DTG curves of P(PA-*alt*-CHO) copolymer derived by the action of Et_2Zn and PPNCl (Et_2Zn/PPNCl/PA/CHO = 2/1/200/200, Table 1 entry 17).